iScience

CellPress
OPEN ACCESS

Article

YTHDF2 favors protumoral macrophage polarization and implies poor survival outcomes in triple negative breast cancer

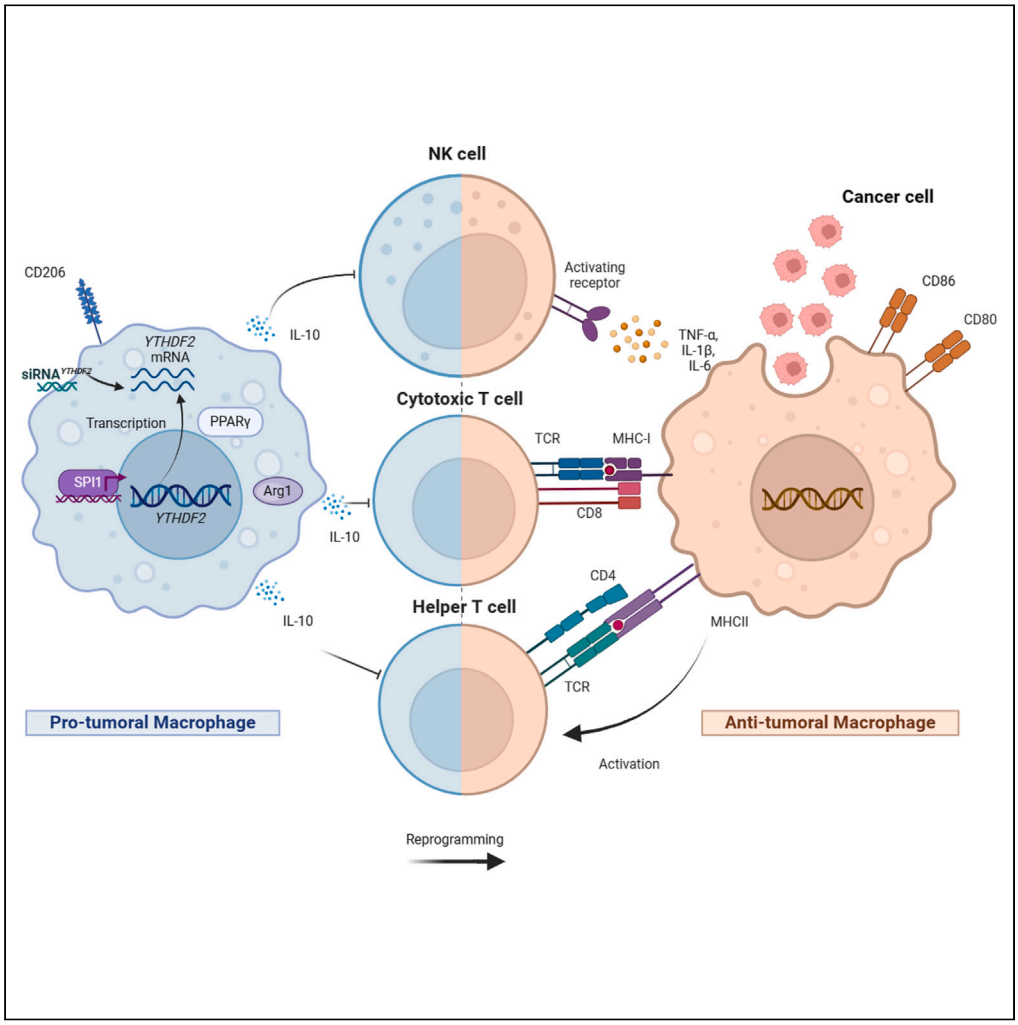

Hao Jin, Yue Chen, Dongbo Zhang, ..., Wen Deng, Jiandong Huang, Yandan Yao

jdhuang@hku.hk (J.H.)
yaoyand@mail.sysu.edu.cn (Y.Y.)

Highlights

m^{6}A reader YTHDF2 was highly expressed in pro-tumoral macrophages

YTHDF2 correlates with pro-tumoral and immuno-suppressing signals of macrophages

Identification of *SPI1* as key transcriptional regulator in *YTHDF2*-high macrophage

Ythdf2 associates with pro-tumoral phenotype polarization of macrophages in the mice

Jin et al., iScience 27, 109902
June 21, 2024
https://doi.org/10.1016/j.isci.2024.109902

iScience

CellPress
OPEN ACCESS

Article

YTHDF2 favors protumoral macrophage polarization and implies poor survival outcomes in triple negative breast cancer

Hao Jin,[1,2,8] Yue Chen,[1,2,8] Dongbo Zhang,[1,2,8] Junfan Lin,[1,2,8] Songyin Huang,[2] Xiaohua Wu,[1,2] Wen Deng,[1,2] Jiandong Huang,[3,4,5,*] and Yandan Yao[1,2,6,7,9,*]

SUMMARY

Patients with triple-negative breast cancer (TNBC) frequently experience resistance to chemotherapy, leading to recurrence. The approach of optimizing anti-tumoral immunological effect is promising in overcoming such resistance, given the heterogeneity and lack of biomarkers in TNBC. In this study, we focused on YTHDF2, an N6-methyladenosine (m^6A) RNA-reader protein, in macrophages, one of the most abundant intra-tumoral immune cells. Using single-cell sequencing and *ex vivo* experiments, we discovered that YTHDF2 significantly promotes pro-tumoral phenotype polarization of macrophages and is closely associated with down-regulated antigen-presentation signaling to other immune cells in TNBC. The *in vitro* deprivation of YTHDF2 favors anti-tumoral effect. Expressions of multiple transcription factors, especially *SPI1*, were consistently observed in *YTHDF2*-high macrophages, providing potential therapeutic targets for new strategies. In conclusion, YTHDF2 in macrophages appears to promote pro-tumoral effects while suppressing immune activity, indicating the treatment targeting YTHDF2 or its transcription factors could be a promising strategy for chemoresistant TNBC.

INTRODUCTION

Triple-negative breast cancer (TNBC) is characterized by the absence of estrogen (ER), progesterone (PR), and human epidermal growth factor (HER-2) receptor expressions, resulting in aggressive behavior and poor prognosis among all subtypes, with limited responses to endocrine and targeted therapies.[1] Consequently, chemotherapy has become the standard clinical practice.[2–5] However, frequent distant metastasis occurs in patients who fail to achieve a complete response (CR) to the treatment,[6–9] necessitating the development of new strategies to overcome resistance and improve CR rates in TNBC. Emerging evidence suggests that chemotherapeutic agents not only exert direct cytotoxic effects but also concurrently activate anti-tumor immune mechanisms, which determine treatment efficacy.[10,11]

The concept of the tumor immune microenvironment (TIME) comprehends the most recent advances achieved in studying the signaling interactions among tumor, stromal and immune cells. Given the lack of biomarkers and extensive heterogeneity in TNBC, the strategy that optimizes anti-tumoral immunity in TIME becomes prospective to overcome such resistance in TNBC.[12–15] Macrophages, as phagocytic cells in the innate immune system, are amongst the most abundant intra-tumoral immune cells. They play a crucial role in the recognition, processing, and degradation of pathogens and tumor cells.[13,16–18] Macrophage polarization refers to the differentiation of two distinct phenotypes based on their functions: the classically activated anti-tumoral phenotype and the alternatively activated pro-tumoral phenotype.[19] Anti-tumoral macrophages are associated with Lipopolysaccharide (LPS) -induced inflammatory cytokines such as interleukin-6 (IL-6), tumor necrosis factor (TNF-α), and interleukin 1β (IL-1β), which have potent anti-cancer properties. In contrast, pro-tumoral macrophages (also known as tumor-associated macrophages, or TAMs) significantly contribute to the unfavorable growth and metastasis of TNBC by releasing angiogenic factors and interleukin-10 (IL-10).[20]

[1]Breast Tumor Center, Sun Yat-sen Memorial Hospital, Sun Yat-sen University, Guangzhou, Guangdong Province 510120, China
[2]Guangdong Provincial Key Laboratory of Malignant Tumor Epigenetics and Gene Regulation, Sun Yat-sen Memorial Hospital, Sun Yat-sen University, Guangzhou, Guangdong Province 510120, China
[3]School of Biomedical Sciences, Li Ka Shing Faculty of Medicine, The University of Hong Kong, Pokfulam, Hong Kong SAR, China
[4]Key Laboratory of Quantitative Synthetic Biology, Shenzhen Institute of Synthetic Biology, Shenzhen Institutes of Advanced Technology, Chinese Academy of Sciences, Shenzhen, Guangdong Province 518055, China
[5]Clinical Oncology Center, Shenzhen Key Laboratory for Cancer Metastasis and Personalized Therapy, The University of Hong Kong-Shenzhen Hospital, Shenzhen, Guangdong Province, China
[6]Shenshan Medical Center, Sun Yat-sen Memorial Hospital, Sun Yat-sen University, Shanwei, Guangdong Province 516621, China
[7]Guangdong Provincial Key Laboratory of Cancer Pathogenesis and Precision Diagnosis and Treatment, Sun Yat-sen Memorial Hospital, Sun Yat-sen University, Shanwei, Guangdong Province 516621, China
[8]These authors contributed equally
[9]Lead contact
*Correspondence: jdhuang@hku.hk (J.H.), yaoyand@mail.sysu.edu.cn (Y.Y.)
https://doi.org/10.1016/j.isci.2024.109902

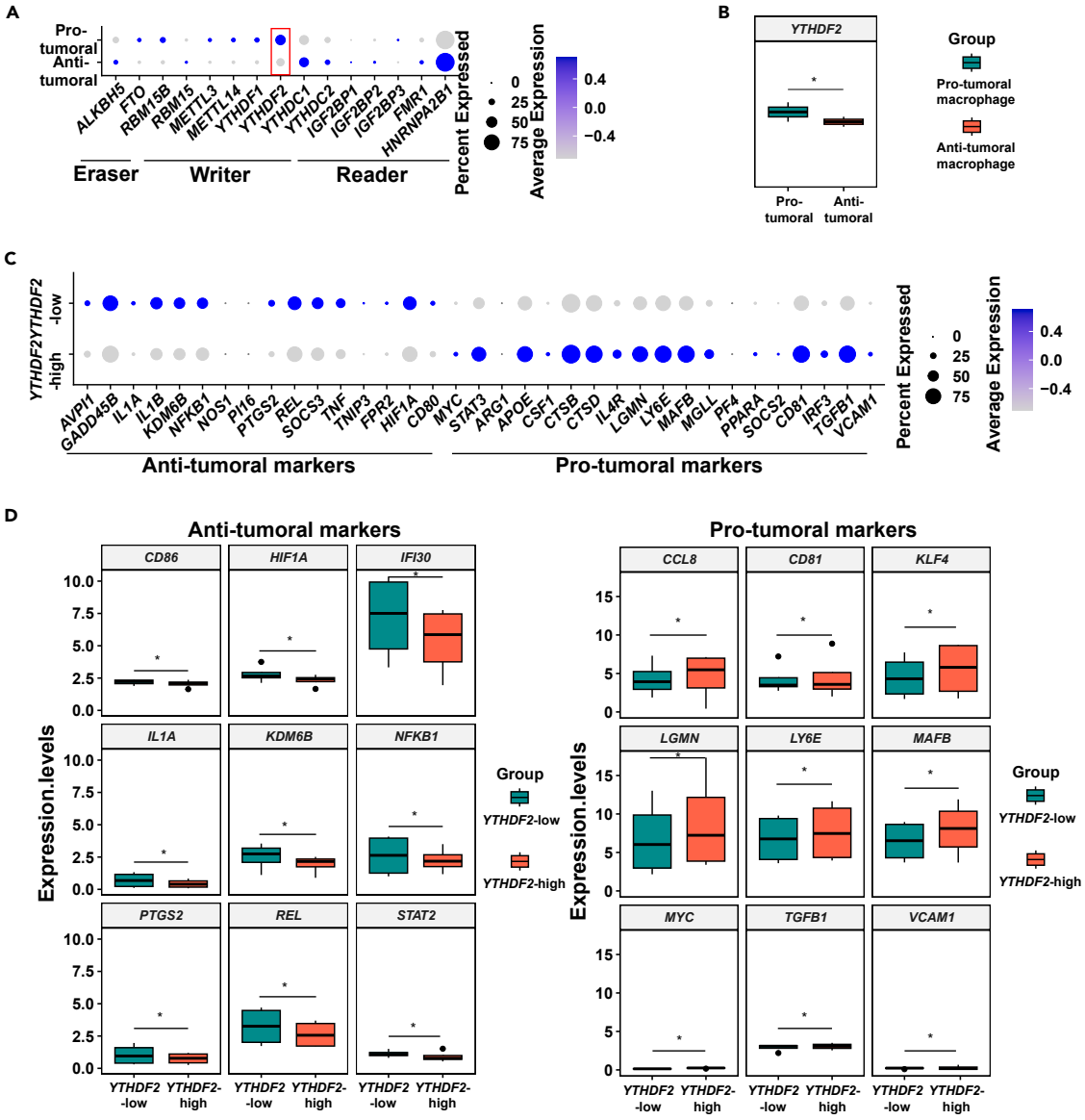

Figure 1. m^{6}A RNA-related protein gene programs associated with anti-tumoral/pro-tumoral macrophages within tumors

(A) Dot plot representing the relative average expression of a subset of m^{6}A-related protein genes (X axis) across anti-tumoral and pro-tumoral clusters (Y axis). The m^{6}A eraser/writer/reader protein genes in each cluster were identified by log fold change compared with the rest. As indicated on the legend, dot size denotes the percentage of cells in a cluster expressing each gene. Dot color represents the relative average expression levels. Red box indicates the relative average expression of YTHDF2.

(B) Normalized expression of *YTHDF2* gene comparing anti-tumoral and pro-tumoral macrophages aggregated by clusters in a pseudo-bulk approach (n = 7 patients, p values calculated by Moses Extreme Reactions test, *$p < 0.05$).

(C) Dot plot representing the relative average expression of a subset of anti-tumoral/pro-tumoral marker genes (X axis) across *YTHDF2*-high and *YTHDF2*-low clusters (Y axis). The anti-tumoral/pro-tumoral marker genes in each cluster were identified by log fold change compared with the rest. As indicated on the legend, dot size denotes the percentage of cells in a cluster expressing each gene. Dot color represents the relative average expression levels.

(D) Normalized expressions of anti-tumoral marker genes comparing *YTHDF2*-high and *YTHDF2*-low macrophages aggregated by clusters in a pseudo-bulk approach (p values calculated by Moses Extreme Reactions test, *$p < 0.05$).

N6-methyladenosine (m^{6}A) is the most abundant epigenetic modification of RNA, and its dysregulation leads to aberrant transcription and translation programs that promote tumorigenesis and cancer progression, closely correlating with macrophage polarization.[21] The principal components involved in modifying m^{6}A are the m^{6}A readers, writers, and erasers. The YTH domain family of m^{6}A readers was first identified by Stoilov P et al. in 2002.[22] Since its first discovery in 2012,[23] YTHDF2, as the m^{6}A reader[21] and regulator of mRNA stability[24] and innate immunity,[25] has been found to correlate with resistance to 5-fluorouracil in colorectal cancer[26] and resistance to cisplatin in ovarian cancer.[27]

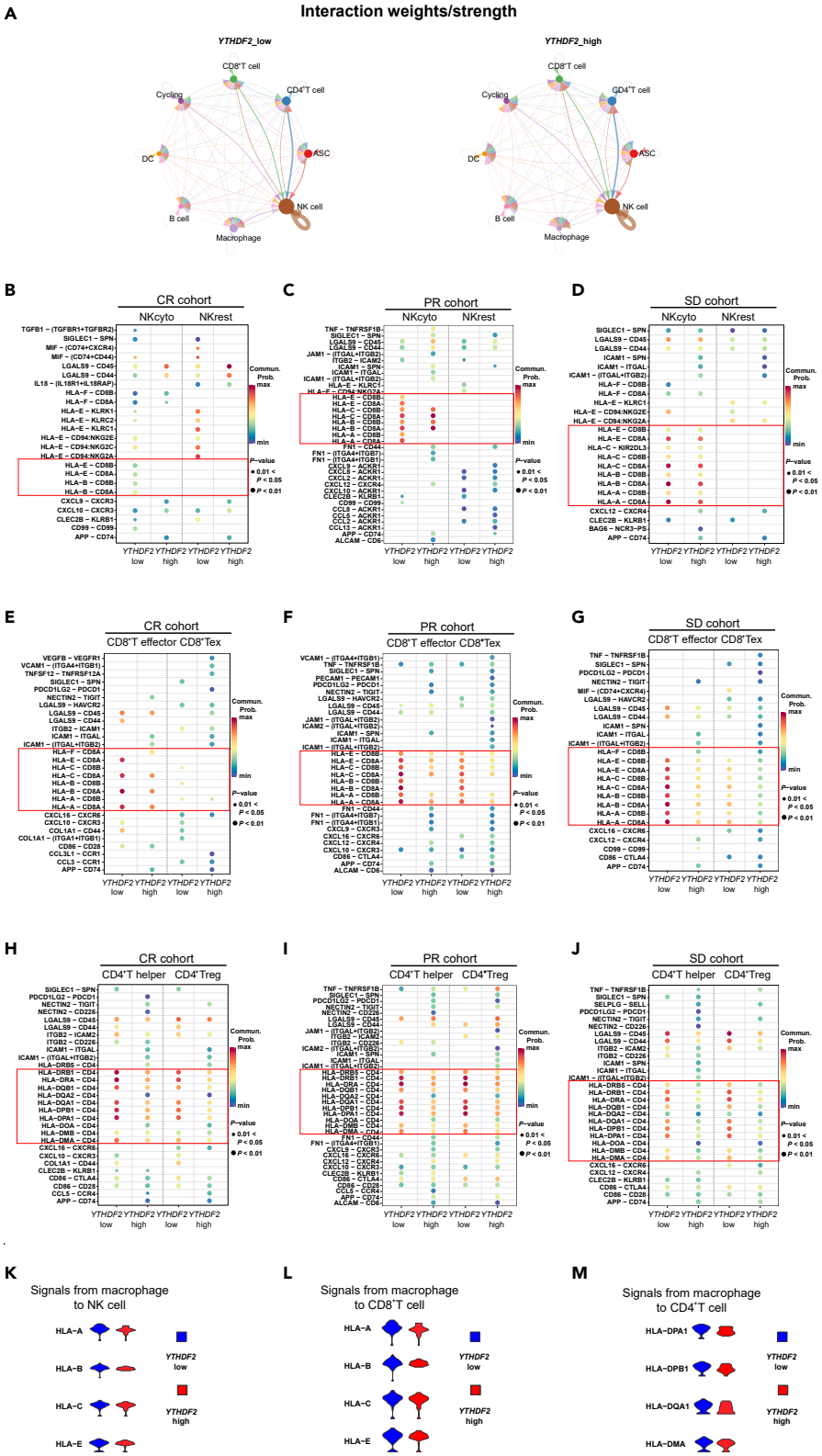
A
Interaction weights/strength
YTHDF2_low
YTHDF2_high
CD8⁺T cell
CD4⁺T cell
Cycling
DC
ASC
NK cell
B cell
Macrophage
B
C
D
CR cohort
PR cohort
SD cohort
NKcyto
NKrest
E
F
G
CD8⁺T effector CD8⁺Tex
H
I
J
CD4⁺T helper
CD4⁺Treg
K
L
M
Signals from macrophage to NK cell
Signals from macrophage to CD8⁺T cell
Signals from macrophage to CD4⁺T cell
HLA-A
HLA-B
HLA-C
HLA-E
HLA-DPA1
HLA-DPB1
HLA-DQA1
HLA-DMA
YTHDF2 low
YTHDF2 high

Figure 2. Expression of receptor-ligand pairs that can mediate interaction between *YTHDF2*-high/*YTHDF2*-low macrophage clusters and NK cell/CD8$^+$ T cell/CD4$^+$ T cell clusters

(A) Circle plot with a correlation analysis on the association of *YTHDF2*-high/*YTHDF2*-low macrophages of all the conditions with all other immune populations, thickness of the lines indicating strength of the interactions.

(B–D) Interactions between *YTHDF2*-high/*YTHDF2*-low macrophage and NK cell clusters in CR (B)/PR (C)/SD (D) cohort.

(E–G) Interactions between *YTHDF2*-high/*YTHDF2*-low macrophage and CD8$^+$ T cell clusters in CR (E)/PR (F)/SD (G) cohort.

(H–J) Interactions between *YTHDF2*-high/*YTHDF2*-low macrophage and CD4$^+$ T cell clusters in CR (H)/PR (I)/SD (J) cohort. B-J: Dot color represents communication probabilities and dot size reflects computed *p* values (one-sided permutation test) for interactions that vary between *YTHDF2*-high and *YTHDF2*-low samples; empty space indicates no difference between two clusters, red boxes indicate decreased immune-activating interactions existing in *YTHDF2*-high macrophage.

(K–M) Violin plot showed the normalized scRNA-seq expression distribution of immune-activating ligand-receptor pairs, compared across NK cells (K)/CD8$^+$ T cells (L)/CD4$^+$ T cells (M) and *YTHDF2*-high/*YTHDF2*-low macrophages.

Previous studies regarding m^{6}A modification have reported the role of *Ythdf2* gene knocking out in inducing anti-tumoral polarization in macrophage, thereby promoting CD8$^+$ T cell-mediated anti-tumoral immunity in MC38 and B16f10 tumor models.[28] Nevertheless, some other articles report an opposing effect that YTHDF2 inhibits the progression of cancer,[29,30] leaving its exact function in TNBC ambiguous.

In this study, we aim to elucidate the role of m^{6}A reader YTHDF2 in the pro-tumoral phenotype polarization in the intra-tumoral macrophages of TNBC, how it alters the signaling of macrophages to other immune cells and possibly transforms TIME, with the goal of identifying new therapeutic targets.

RESULTS

Identification of anti-/pro-tumoral macrophages in TNBC tumor specimens

Tumor-infiltrating macrophages (Mφ) of all the conditions partitioned to two sub-clusters, respectively representing anti-tumoral Mφ and pro-tumoral Mφ. Previous studies revealed that in the macrophages against tumor cells, anaerobic glucose metabolism was quite principal, while oxidative glucose consumption was dominant in pro-tumoral macrophages.[31,32] In addition, the levels of the components in mitochondrial TCA cycles, such as fumarate, succinate and itaconate also competently guide the activation of macrohages.[33] Macrophage phagocytosis is triggered by a comprehensive signaling network including the involvements of GTPases, lipids, protein kinases, phosphatases and actin regulatory proteins.[34,35] They drive the formation, internalization and disposition of macropinsosome.[36] We hereby aimed to target the relevant genes that represented dysregulated metabolism and phagocytosis in macrophages to define the pro-tumoral signature, whereas those related to immune enhancement were used to define the anti-tumoral signature.

A total of 28,547 CD45$^+$ cells, 17,854 CD45$^+$ cells, and 32,564 CD45$^+$ cells in tumor specimens respectively from TNBC patients achieving complete response (CR), partial response (PR), or stable disease (SD) after chemotherapy were subjected to clustering analysis (Figure S1). We subclustered the CD45$^+$ immune cells and a total of 1,152 cells, 873 cells, and 1,240 cells in macrophage/monocyte population were identified respectively in the CR, PR and SD cohort. Macrophages were distinguished from monocytes to the utmost effort.

The cluster anti-tumoral Mφ and cluster pro-tumoral Mφ were distinguished by the alternative expressions of *APOE*/*CD163*/*LGMN*/*CTSD* versus *IL1A*/*IL1B*/*TNF*/*NFKB1* respectively (Figures S2A and S2B). We next identified differentially expressed (DE) genes between pro-tumoral and anti-tumoral tumor-infiltrating macrophages. Pro-tumoral marker genes were shown to be upregulated in pro-tumoral Mφ, including *APOE*, *CTSD*, *LGMN*, and *CD163*, whereas upregulated genes in anti-tumoral macrophages included genes previously identified in human anti-tumoral macrophages, including *IL1B*, *NFKB1*, *IL1A*, and *TNF* (Figure S2C).[37,38] We further investigated the subpopulation-specific transcriptional signatures across the two clusters. Consistent with the results of the DE genes analysis, cluster anti-tumoral Mφ highly expressed marker genes such as *IL1A*, *IL1B*, *NFKB1*, *NOS1*, *REL*, and *TNF*, while cluster pro-tumoral Mφ displayed higher level of *MRC1*, *LGMN*, *CTSD*, and *CD163* (Figure S2D). In a similar manner, Gene Set Enrichment Analyses (GSEA) including Gene Ontoloty (GO), Reactome, and Kyoto Encyclopedia of Genes and Genomes (KEGG) confirmed significant activities of immune-activating signaling pathways in anti-tumoral macrophages rather than in pro-tumoral macrophages, such as positive cytokine regulation, cellular response to stimulus, multiple Toll-like receptor cascades and other signaling pathways (Figures S2E, S2G, and S2I). In contrast, pro-tumoral macrophages showed a tendency of having alternative metabolic and endocytic pathways like lipoprotein, cholesterol and glycan utilization, as well as receptor-mediated endocytosis and transferrin recycling, etc. (Figures S2F, S2H, and S2J).

The two robust subclusters, cluster anti-tumoral Mφ and cluster pro-tumoral Mφ, represented different distributions of pre-treatment macrophages and post-treatment macrophages (Figure S3A). Pseudotime analysis identified one major trajectory, composed of cells from *APOE*$^+$ cluster pro-tumoral macrophages and *IL1A*$^+$ cluster anti-tumoral macrophages (Figure S3B). Comparison of matched pre- and post-treatment specimens demonstrated a post-treatment increase trend in the percentage of anti-tumoral macrophages, especially in CR cohort (Figures S3C–S3E).

m^{6}A reader YTHDF2 is highly expressed in pro-tumoral macrophages

The notable expression of YTHDF2, compared to other proteins in m^{6}A readers, was consistently observed in pro-tumoral macrophages across all cohorts (Figures 1A, 1B, and S3F). On the other hand, high expression levels of anti-tumoral macrophage markers were prominent in the *YTHDF2*-low group, and quite the opposite situation occurred in terms of pro-tumoral macrophage markers in the *YTHDF2*-high group (Figures 1C and 1D). This demonstrated the positive correlation between YTHDF2 expression and pro-tumoral macrophages.

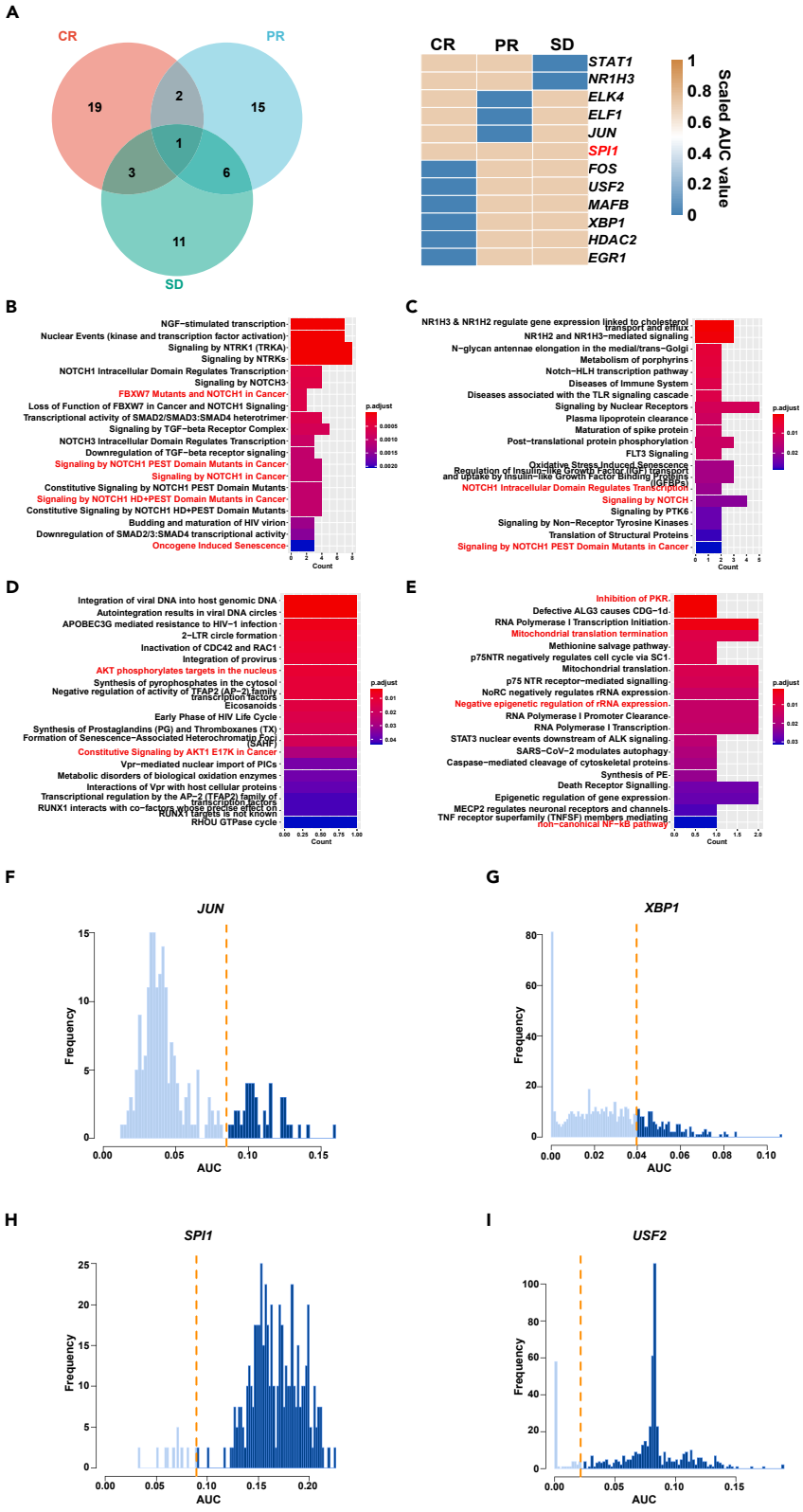
A
CR
PR
SD
19
2
15
1
3
6
11
CR PR SD
STAT1
NR1H3
ELK4
ELF1
JUN
SPI1
FOS
USF2
MAFB
XBP1
HDAC2
EGR1
Scaled AUC value
1
0.8
0.6
0.4
0.2
0
B
NGF−stimulated transcription
Nuclear Events (kinase and transcription factor activation)
Signaling by NTRK1 (TRKA)
Signaling by NTRKs
NOTCH1 Intracellular Domain Regulates Transcription
Signaling by NOTCH3
FBXW7 Mutants and NOTCH1 in Cancer
Loss of Function of FBXW7 in Cancer and NOTCH1 Signaling
Transcriptional activity of SMAD2/SMAD3:SMAD4 heterotrimer
Signaling by TGF−beta Receptor Complex
NOTCH3 Intracellular Domain Regulates Transcription
Downregulation of TGF−beta receptor signaling
Signaling by NOTCH1 PEST Domain Mutants in Cancer
Signaling by NOTCH1 in Cancer
Constitutive Signaling by NOTCH1 PEST Domain Mutants
Signaling by NOTCH1 HD+PEST Domain Mutants in Cancer
Constitutive Signaling by NOTCH1 HD+PEST Domain Mutants
Budding and maturation of HIV virion
Downregulation of SMAD2/3:SMAD4 transcriptional activity
Oncogene Induced Senescence
p.adjust
Count
C
NR1H3 & NR1H2 regulate gene expression linked to cholesterol transport and efflux
NR1H2 and NR1H3−mediated signaling
N−glycan antennae elongation in the medial/trans−Golgi
Metabolism of porphyrins
Notch−HLH transcription pathway
Diseases of Immune System
Diseases associated with the TLR signaling cascade
Signaling by Nuclear Receptors
Plasma lipoprotein clearance
Maturation of spike protein
Post−translational protein phosphorylation
FLT3 Signaling
Oxidative Stress Induced Senescence
Regulation of Insulin−like Growth Factor (IGF) transport and uptake by Insulin−like Growth Factor Binding Proteins (IGFBPs)
NOTCH1 Intracellular Domain Regulates Transcription
Signaling by NOTCH
Signaling by PTK6
Signaling by Non−Receptor Tyrosine Kinases
Translation of Structural Proteins
Signaling by NOTCH1 PEST Domain Mutants in Cancer
p.adjust
Count
D
Integration of viral DNA into host genomic DNA
Autointegration results in viral DNA circles
APOBEC3G mediated resistance to HIV−1 infection
2−LTR circle formation
Inactivation of CDC42 and RAC1
Integration of provirus
AKT phosphorylates targets in the nucleus
Synthesis of pyrophosphates in the cytosol
Negative regulation of activity of TFAP2 (AP−2) family transcription factors
Eicosanoids
Early Phase of HIV Life Cycle
Synthesis of Prostaglandins (PG) and Thromboxanes (TX)
Formation of Senescence−Associated Heterochromatic Foci (SAHF)
Constitutive Signaling by AKT1 E17K in Cancer
Vpr−mediated nuclear import of PICs
Metabolic disorders of biological oxidation enzymes
Interactions of Vpr with host cellular proteins
Transcriptional regulation by the AP−2 (TFAP2) family of transcription factors
RUNX1 interacts with co−factors whose precise effect on RUNX1 targets is not known
RHOU GTPase cycle
p.adjust
Count
E
Inhibition of PKR
Defective ALG3 causes CDG−1d
RNA Polymerase I Transcription Initiation
Mitochondrial translation termination
Methionine salvage pathway
p75NTR negatively regulates cell cycle via SC1
Mitochondrial translation
p75 NTR receptor−mediated signalling
NoRC negatively regulates rRNA expression
Negative epigenetic regulation of rRNA expression
RNA Polymerase I Promoter Clearance
RNA Polymerase I Transcription
STAT3 nuclear events downstream of ALK signaling
SARS−CoV−2 modulates autophagy
Caspase−mediated cleavage of cytoskeletal proteins
Synthesis of PE
Death Receptor Signalling
Epigenetic regulation of gene expression
MECP2 regulates neuronal receptors and channels
TNF receptor superfamily (TNFSF) members mediating non−canonical NF−κB pathway
p.adjust
Count
F
JUN
Frequency
AUC
G
XBP1
Frequency
AUC
H
SPI1
Frequency
AUC
I
USF2
Frequency
AUC

Figure 3. Identification of SPI1 TFs Regulating *YTHDF2*-High Macrophages in CR, PR, and SD cohorts, respectively

(A) (left) Venn diagram showing the shared TFs for *YTHDF2*-high macrophages of the 3 indicated cohorts of comparisons and (right) heatmap showing scaled AUC value of the TFs shared by 2 or more indicated cohorts.

(B–E) GSEA (hypeR) based on REACTOME for genes in macrophages regulated by the specific TF *EGR1* (B), TF *NR1H3* (C), TF *MAFB* (D), and TF *HDAC2* (E). Red indicates immune-suppressive and tumor-promoting signaling pathway.

(F–I) AUC histograms of some specific TF *JUN* (F), TF *XBP1* (G), TF *SPI1* (H), and TF *USF2* (I) for *YTHDF2*-high macrophages (red line indicates threshold).

YTHDF2 positively correlates with pro-tumoral and immuno-suppressive signal transduction between macrophages and other immune cells

By performing a correlation analysis on the association of *YTHDF2*-high/*YTHDF2*-low macrophages of all the conditions with immune populations, we found the significantly correlated populations are NK cells, $CD4^+$ T cells and $CD8^+$ T cells (Figure 2A). We first examined how YTHDF2 levels influenced the interactions between macrophages and natural killer (NK) cells in all three cohorts. NK cells consisted of cytotoxic (NKcyto) and resting NK cells (NKrest), distinguished by their alternative functions.[39,40] Similarly, $CD8^+$ T cells consisted of effector T cells (Tem, highly expressing effector and cytotoxic markers) and exhaustion-like T cells (Tex, highly expressing immune-checkpoint markers).[37] The results showed that lower expression of macrophage YTHDF2 was associated with stronger immune-activating interactions with NK cells and $CD8^+$ T cells. Multiple antigen-presentation signals were involved in these interactions, such as signals derived from major histocompatibility complex (MHC) class I molecules, including human leukocyte antigen (HLA)-E, HLA-A, HLA-B, and HLA-C, which serve as ligands for CD8A and CD8B receptors (Figures 2B–2G, 2K, and 2L).[41,42]

Next, we performed analogous comparisons between $CD4^+$ T cells and *YTHDF2*-high/*YTHDF2*-low macrophages. The results showed that multiple immune-activating signals were enriched in *YTHDF2*-low macrophages, including signals derived from MHC class II molecules, including HLA-DMA, HLA-DMB, HLA-DOA, HLA-DPA1, HLA-DPB1, HLA-DQA1, HLA-DQA2, HLA-DQB1, HLA-DRA, HLA-DRB1, and HLA-DRB5, which serve as ligands for CD4 receptor (Figures 2H–2J, and 2M).[43,44]

Identification of *SPI1* transcription factors regulating *YTHDF2*-high macrophages

A total of 199 transcription factors (TFs), 203 TFs, and 182 TFs in charge of macrophage infiltration were identified in CR, PR, and SD cohorts, respectively. After scaling the area under curve (AUC) values and obtained binary AUC matrix of these TFs, we identified 25 TFs, 24 TFs, and 21 TFs of CR/PR/SD cohort in *YTHDF2*-high group macrophages (Figures 3A and S4–S6). A total of 12 TFs were shared by two or more cohorts, including *STAT1*, *NR1H3*, *ELK4*, *ELF1*, *JUN*, *SPI1*, *FOS*, *USF2*, *MAFB*, *XBP1*, *HDAC2*, and *EGR1*, wherein the TF *SPI1* was shared by all three cohorts and regulated a largest number of genes (279 genes in CR cohort, 203 genes in PR cohort, and 96 genes in SD cohort) (Figures 3A and S4–S6). As a conclusion, it is likely that *SPI1* has unique significance in the generation of *YTHDF2*-high macrophages.

The transcriptional spectra regulated by the twelve TFs were highly overlapped. We used REACTOME to analyze their scopes of regulation in terms of cellular metabolism, immunity and macrophages. It could be seen that *EGR1* participated in tissue injury, immune response, fibrosis and macrophage migration inhibition via FBXW7 and NOTCH1 (Figure 3B).[45,46] *NR1H3* was key to lipid homeostasis, anti-inflammatory and pro-tumoral response in macrophages via NOTCH1 as well (Figure 3C).[46,47] *MAFB* worked through AKT phosphorylation to influence monocyte proliferation and its differentiation to macrophages (Figure 3D).[48,49] *HDAC2* broadly involved in multiple transcriptional modulations such as PKR inhibition, NF-kB signaling and mitochondrial translation termination (Figure 3E).[50–53] *SPI1* committed macrophage maturation and reprogramming by ROBO signaling pathway (Figure S7A).[54–56] *XBP1* favored the synthesis and secretion of cholesterol to cause immunosuppression, as well as regulating pro-tumoral macrophages signaled by WNT in cancer (Figure S7B).[57–59] The rest of the TFs also presented similar patterns (Figures S7C–S7H). Despite most of the identified TFs had been reported to involve in macrophage differentiation or polarization, their specific roles in *YTHDF2* gene transcription had yet been well explored.

The AUC activity score analyses verified significant involvements of the factors in the *YTHDF2*-high macrophages (the threshold lines highlight cells in which TFs have the highest activity scores) (Figures 3F–3I). Overall, the above results showed that these TFs may play a critical role in the transcription of YTHDF2 in intra-tumoral macrophages of TNBC.

Ythdf2 expression associates with pro-tumoral phenotype polarization in the mice bone marrow-derived macrophages

To verify the effect of YTHDF2 on macrophage polarization, we designed three siRNA sequences to suppress *Ythdf2* expression in the mice bone marrow-derived macrophages (BMDM) (Table S1). As shown in Figure S8, siRNA treatment significantly hindered *Ythdf2* gene transcription. Especially, $siRNA^{Ythdf2}$-2 had the highest knocking-out rate and was used for the following experiment. We then assessed the expressions of anti-tumoral/pro-tumoral phenotype marker genes in BMDMs after the excision of *Ythdf2* based on this *ex vivo* macrophage polarization model. *Ythdf2*-silenced macrophages were subjected to LPS or IL-4 treatment for 12 h to induce macrophage polarization. Flow cytometry was applied to confirm the establishment of pro-tumoral/anti-tumoral macrophage (Figure S9). Quantitative PCR (qPCR) (Table S2) analyses were used to validate the transcriptions of anti-tumoral/pro-tumoral phenotype marker genes by measuring the levels of mRNAs. Notably, the cellular expressions of anti-tumoral markers such as *Il1b*, *Il6*, and *Tnfα* in *Ythdf2*-silenced macrophages surpassed those in the control group (Figure 4A); quite the opposite circumstances were seen regarding the pro-tumoral markers, including *Arg1*, *Il10*, and *Ppapγ* (Figure 4B). The results of flow cytometry showed that the percentages of $Cd80^+$ or $Cd86^+$ cells were higher in $siRNA^{Ythdf2}$ group than in control group (Figures 4C and 4D), whereas the percentage of $Cd206^+$ cells were higher in control group than in $siRNA^{Ythdf2}$

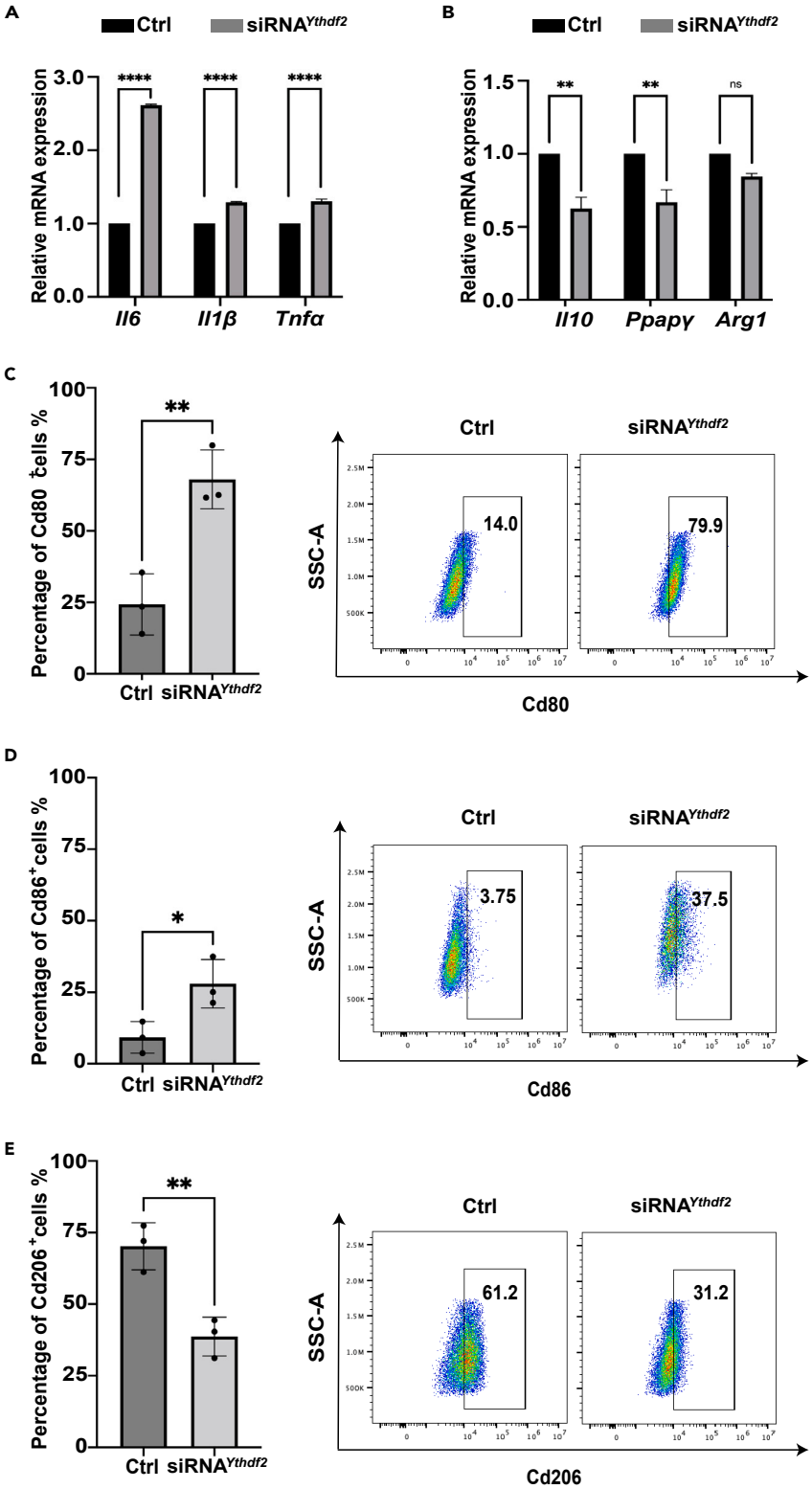

Figure 4. *Ythdf2* expression positively correlates with the expressions of pro-tumoral markers in BMDMs

(A) BMDMs were treated with 1 μg/mL LPS for 12 h to generate anti-tumoral macrophages. Expressions of *Il6*, *Il1β*, and *Tnf α* in anti-tumoral BMDMs with or without siRNA^{Ythdf2} treatment (two-sided t-test, ****$p < 0.0001$).

Figure 4. *Continued*

(B) BMDMs were treated with 20 ng/mL murine IL-4 for 12 h to generate pro-tumoral macrophages. Expression of *Il10*, *Ppapγ* and *Arg1* in pro-tumoral BMDMs with or without siRNA^{Ythdf2} treatment (two-sided t-test, $^{**}p < 0.01$).

(C–E) Representative plots and percentages of Cd80^{+} (C) or Cd86^{+} (D) or Cd206^{+} (E) BMDMs from control and siRNA^{Ythdf2} group after LPS (C, D) or IL-4 (E) treatment ($n = 3$, two-tailed t-test, $^{*}p < 0.05$, $^{**}p < 0.01$).

group (Figure 4E). From another perspective, the fact that the knocking out of *Ythdf2* promotes expression of anti-tumoral phenotype marker genes suggested a close connection between this protein and the differentiation of pro-tumoral macrophages.

YTHDF2 associated with tumor growth signaling and reduced anti-tumoral activity in macrophages

Lastly, we analyzed the mutual signaling between macrophages and tumor cells. Compared with *YTHDF2*-low macrophages, *YTHDF2*-high macrophages exhibited pro-tumoral characteristics with multiple malignancy-promoting signals involved, such as RARRES2, MDK-SDC4/SDC2, CX3CL1-CX3CR1, COL4A5, COL4A2, COL4A1, C3AR1, TNFRSF1A, LILRB1, CCL5, ITGAV, SDC4, CD36, CD47, NRP1, and NRP2 (Figures 5A–5C).[60–71] In particular, some prominent pro-tumoral molecules[31] including MSR1, CCL18, STAB1, CD163L1, MERTK, AXL, GPNMB, and CHI3L1 were highly expressed by *YTHDF2*-high macrophages while some prominent anti-tumoral ones[31] including IL1B, CCL2, CCL3, CCL4, TNF, CXCL2, and SOCS3 were highly expressed by *YTHDF2*-low macrophages (Figure 5D). In summary, our observations demonstrate the pro-tumoral tendency of *YTHDF2*-high macrophages.

We also testified the interaction between macrophages and cancer cells *in vivo* by using siRNA^{Ythdf2} to silence the gene expression. The results showed that knocking-out of *Ythdf2* in BMDMs affect macrophage phagocytosis and tumor cell apoptosis, as the phagocytosis by macrophages and apoptosis rates of EMT6 cells were higher in the siRNA^{Ythdf2} group than that in the control group (Figures 5E and 5F). The mean fluorescence intensity (MFI) of carboxyfluorescein succinimidyl ester (CFSE) decreases as cells proliferate. The MFI of CFSE^{+} EMT6 cells in the siRNA^{Ythdf2} group was higher than that in the control group after co-incubation for respectively 12 h and 24 h, indicating lower proliferation rates of EMT6 cells in the siRNA^{Ythdf2} group (Figure 5G). It is hereby concluded that the silencing of YTHDF2 mostly reduces the pro-tumoral signaling while enhancing the anti-tumoral activities conducted by macrophages.

YTHDF2 predicts the PFS of patients with TNBC in TCGA dataset

By subjecting 142 TNBC patients from the TCGA dataset to survival analyses (Figure 6A), we found that the YTHDF2 geneset negatively correlated with the progression-free survival (PFS) of the whole cohort (Figure 6B). Other demographics, such as the age $\geq$40 years old (Figure 6C), age <65 years old (Figure 6D), tumor T1/2/3 (Figure 6E), lymph node metastasis (Figure 6F), no distant metastasis (Figure 6G), and Stage I/II/III (Figure 6H) subgroups also presented similar trends.

DISCUSSION

The understanding of the triggering mechanisms behind pro-tumoral polarization of macrophages by YTHDF2 would enable us to develop new therapeutic strategies for TNBC patients by enhancing tumor-suppressive roles of macrophages. In this study, with the implementation of single-cell sequencing, we demonstrated that YTHDF2 favored the expressions of pro-tumoral macrophage markers and vice versa in terms of anti-tumoral macrophage markers in both chemo-responsive and chemo-resistant patients with TNBC. In addition, *ex vivo Ythdf2* knocking-out experiments and qPCR outcomes indicated that the deprivation of *Ythdf2* expression in the BMDMs exhibited significant preference for anti-tumoral phenotype polarization of macrophages. We also found that *YTHDF2*-high macrophages produce an indirect pro-tumoral immunity via eliciting weaker immune-activating effects on NK/CD8^{+} T/CD4^{+} T cells (signals derived from MHC class I molecules, including HLA-E, HLA-A, HLA-B, and HLA-C, and signals derived from MHC class II molecules, including HLA-DMA, HLA-DMB, HLA-DOA, HLA-DPA1, HLA-DPB1, HLA-DQA1, HLA-DQA2, HLA-DQB1, HLA-DRA, HLA-DRB1, HLA-DRB5) and simultaneously a direct pro-tumoral immunity via eliciting resounding tumor-promotive effects on tumor cells (signals such as RARRES2, MDK-SDC4/SDC2, CX3CL1-CX3CR1, COL4A5, COL4A2, COL4A1, C3AR1, TNFRSF1A, LILRB1, CCL5, ITGAV, SDC4, CD36, CD47, NRP1, and NRP2). The proliferation and metastasis of TNBC are thus likely to be substantially regulated by these interactions.

Our analyses also unraveled a transcriptional regulating network for macrophages in TNBC and discovered some key TFs inside *YTHDF2*-high macrophages. A total of 12 TFs were shared by two or more cohorts, including *STAT1*, *NR1H3*, *ELK4*, *ELF1*, *JUN*, *FOS*, *USF2*, *MAFB*, *XBP1*, *HDAC2*, and *EGR1*. Especially, the TF *SPI1* was common in all three cohorts (CR/PR/SD) and regulated the largest number of genes. Annotation analyses revealed them contributing to the infiltration, status and functionality maintenance of pro-tumoral macrophage. These results indicated that the *YTHDF2*-high signatures we established capture common patterns of intra-tumoral macrophage transcriptional heterogeneity across TNBC. This work reveals a unique resource providing a comprehensive single-cell transcriptome atlas of the macrophage of TNBC, laying a new foundation for the development of precision therapies in TNBC, such as transcription factor inhibitors or conjugated strategies.

Our results from the survival analyses of TNBC patients from TCGA dataset are consistent with the conclusions of previous studies that high levels of YTHDF2 reflect poor prognosis in cancer.[72,73] The finding that the inhibition of YTHDF2 generally evokes an anti-tumoral response also matches with other studies.[26–28] No study regarding the clinical safety and efficacy of YTHDF2 inhibitors had been conducted yet, owing to the contradictory outcomes it brings (both beneficial and detrimental).[29] This is likely due to the shared binding sites of YTHDF2 on different genes; its roles in other immune cells, like B cells, are to be determined.[28,30] Therefore, the possibility has to be taken into consideration that YTHDF2 inhibitors may display alternative overall effects in different cancer types and patients. Further investigations are essential for verification in TNBC.

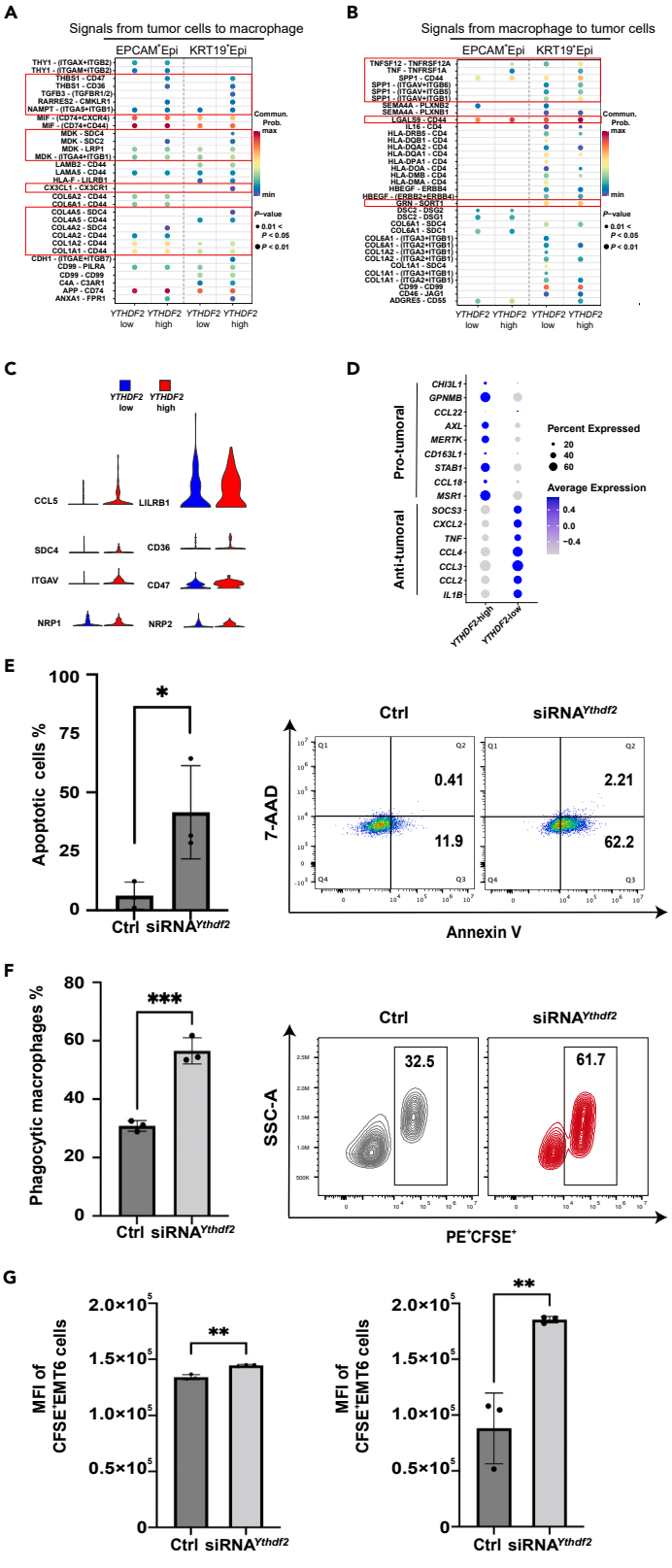
A
Signals from tumor cells to macrophage
EPCAM+Epi
KRT19+Epi
Commun. Prob.
max
min
P-value
0.01 < P < 0.05
P < 0.01
YTHDF2 low
YTHDF2 high
B
Signals from macrophage to tumor cells
C
CCL5
LILRB1
SDC4
CD36
ITGAV
CD47
NRP1
NRP2
D
Pro-tumoral
Anti-tumoral
CHI3L1
GPNMB
CCL22
AXL
MERTK
CD163L1
STAB1
CCL18
MSR1
SOCS3
CXCL2
TNF
CCL4
CCL3
CCL2
IL1B
Percent Expressed
Average Expression
YTHDF2-high
YTHDF2-low
E
Apoptotic cells %
Ctrl
siRNAYthdf2
7-AAD
Annexin V
0.41
11.9
2.21
62.2
F
Phagocytic macrophages %
SSC-A
PE+CFSE+
32.5
61.7
G
MFI of CFSE+EMT6 cells

Figure 5. YTHDF2 associated with tumor growth signaling and treatment with siRNA^{Ythdf2} promotes the anti-tumoral activities conducted by macrophages

(A and B) Expression of receptor-ligand pairs that can mediate interactions between *YTHDF2*-high/*YTHDF2*-low macrophage clusters and tumor cell clusters in CR cohort (A: ligand from tumor cells and receptor on macrophages; B: ligand from macrophages and receptor on tumor cells.). Dot color represents communication probabilities and dot size reflects computed *p* values (one-sided permutation test) for interactions that vary between *YTHDF2*-high and *YTHDF2*-low samples; empty space indicates no difference between two clusters, red boxes indicate increased tumor-promotive interactions existing in *YTHDF2*-high macrophage.

(C) Violin plot showed the normalized scRNA-seq expression distribution of tumor-promotive ligand-receptor pairs, compared across tumor cells and *YTHDF2*-high/*YTHDF2*-low macrophages of CR cohort.

(D) Dot plot representing the relative average expression of a selected subset of pro-tumoral/anti-tumoral marker genes (Y axis) across *YTHDF2*-high and *YTHDF2*-low clusters (X axis). The anti-tumoral/pro-tumoral marker genes in each cluster were identified by log fold change compared with the rest. As indicated on the legend, dot size denotes the percentage of cells in a cluster expressing each gene. Dot color represents the relative average expression levels.

(E) Cell apoptosis (right) and quantitative analysis of cell apoptosis (left) after siRNA^{Ythdf2} treatments (two-sided t test, $*p < 0.05$).

(F) Macrophage phagocytosis (right) and quantitative analysis of macrophage phagocytosis (left) after siRNA^{Ythdf2} treatments (two-sided t test, $*p < 0.05$, $**p < 0.01$, $***p < 0.001$).

(G) Quantitative analysis of MFI of CFSE^{+}EMT6 cells after co-incubation for respectively 12 h (left) and 24 h (right) (two-sided t test, $*p < 0.05$, $**p < 0.01$).

In conclusion, our results suggest that the m^{6}A reader YTHDF2 is a decisive factor in the induction of pro-tumoral-phenotype polarization in the macrophages of TNBC. A *SPI1*-centered transcriptional network systemically facilitates the maintenance of *YTHDF2*-high macrophages in status. The single-cell sequencing analyses revealed that YTHDF2-mediated pro-tumoral macrophages conferred weaker antigen-presentation signals to other immune cells (signals derived from MHC class I molecules, including HLA-E, HLA-A, HLA-B, and HLA-C, and signals derived from MHC class II molecules, including HLA-DMA, HLA-DMB, HLA-DOA, HLA-DPA1, HLA-DPB1, HLA-DQA1, HLA-DQA2, HLA-DQB1, HLA-DRA, HLA-DRB1, HLA-DRB5) and malignancy-promoting signals (such as RARRES2, MDK-SDC4/SDC2, CX3CL1-CX3CR1, COL4A5, COL4A2, COL4A1, C3AR1, TNFRSF1A, LILRB1, CCL5, ITGAV, SDC4, CD36, CD47, NRP1, and NRP2) to tumor cells. Some of the TFs, such as *STAT1*, *NR1H3*, *ELK4*, *ELF1*, *JUN*, *FOS*, *USF2*, *MAFB*, *XBP1*, *HDAC2*, and *EGR1*, and especially *SPI1*, were common and deeply involved in the regulation of those immune-suppressing interactions. YTHDF2 also corresponded to poor progression-free survival rates in our analyses of the TNBC samples in TCGA dataset. Future experiments would ideally consist of larger-scaled samples, *in vivo* models, physiopathological investigation, documentation of the m^{6}A status of the target polarization transcripts, and participants receiving immunotherapy. We sincerely hope that our findings could provide new insights to spark inspirational thoughts in the clinical applications of YTHDF2 or relative transcription factor inhibitors.

Limitations of the study

This study emphasizes the roles of YTHDF2 in affecting pro-tumoral-phenotype macrophage polarization and predicting prognosis in TNBC. However, there were some limitations when reviewing the whole experiments. First, the patients who achieved CR were treated with doxorubicin-based regimen, whereas the patients with PR or SD were treated with paclitaxel regimen. Even though research has shown that both doxorubicin and paclitaxel could induce immunogenic death of tumor cell[74,75] and correlate with macrophage activation,[76,77] the alternative anti-cancer mechanisms of these two drugs may render any conclusion regarding treatment response unpersuasive. Future trials will be required to unify the regimen so to achieve convincing conclusions associated with response. Second, we did not test our observations in *in vivo* models, nor were the outcomes of YTHDF2 inhibitors examined. Moreover, a larger scaled sample pool, if possible, would make our conclusions more persuasive. The role of YTHDF2 gene in the physiopathological process of macrophages has not been thoroughly investigated. The probability of other mechanisms, other than post-translational m^{6}A modifications, being determinative to the pro-tumoral polarization of macrophages cannot be completely excluded. A comprehensive network taking all the transcriptional components into account is necessary to verify such a statement. The role of YTHDF2 in anti-tumoral and pro-tumoral macrophages, and differentially expressed immune signaling pathways in the two classes will be more convincing if those patients enrolled in this study were treated with immunotherapy.

STAR★METHODS

Detailed methods are provided in the online version of this paper and include the following:

- KEY RESOURCES TABLE
- RESOURCE AVAILABILITY
  - Lead contact
  - Materials availability
  - Data and code availability
- EXPERIMENTAL MODEL AND STUDY PARTICIPANT DETAILS
  - Animal subjects
  - Human subjects
- METHOD DETAILS
  - Patients and sample collection
  - Cell culture and macrophage polarization

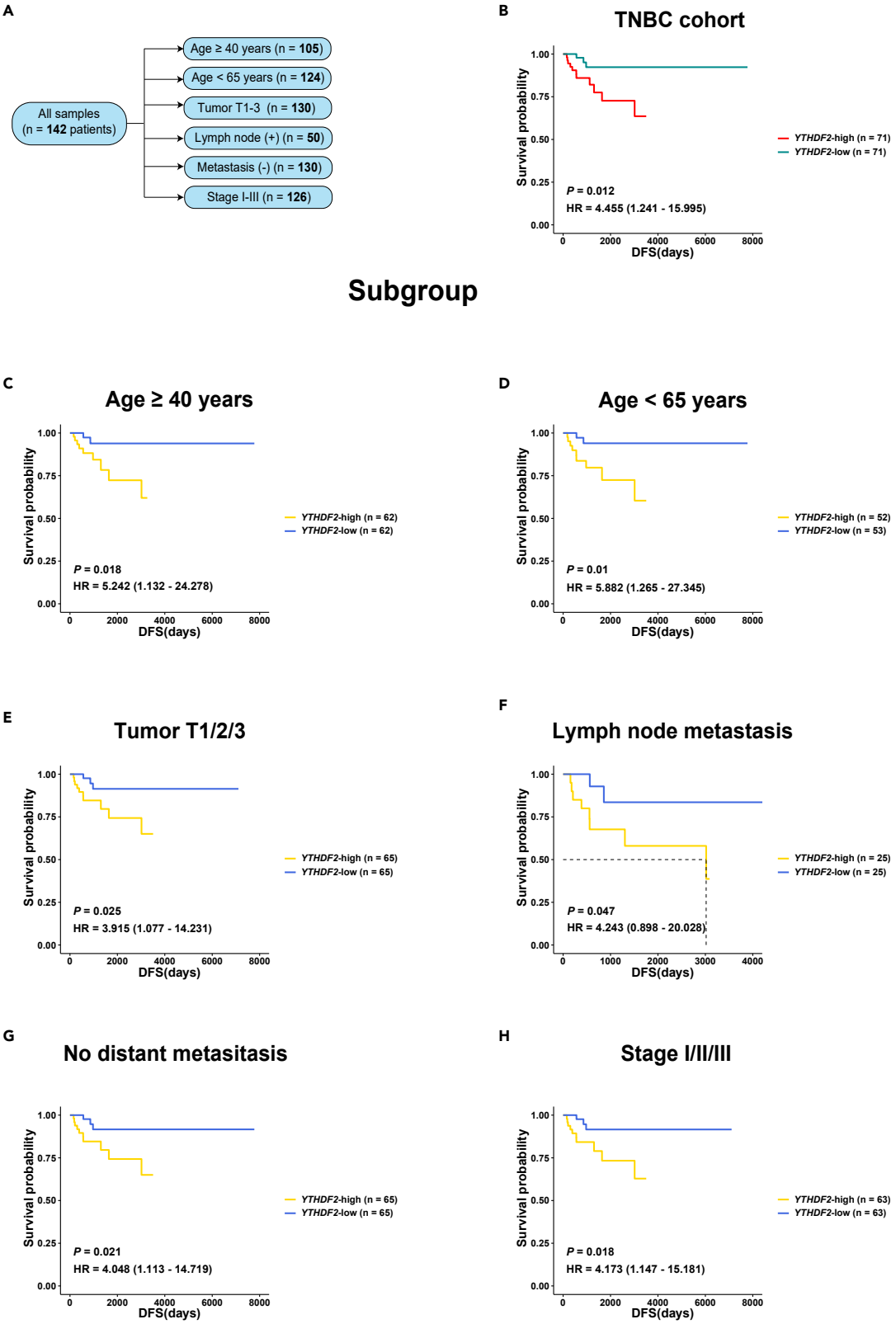
A
All samples
(n = 142 patients)
Age ≥ 40 years (n = 105)
Age < 65 years (n = 124)
Tumor T1-3 (n = 130)
Lymph node (+) (n = 50)
Metastasis (-) (n = 130)
Stage I-III (n = 126)
B
TNBC cohort
Survival probability
DFS(days)
P = 0.012
HR = 4.455 (1.241 - 15.995)
YTHDF2-high (n = 71)
YTHDF2-low (n = 71)
Subgroup
C
Age ≥ 40 years
P = 0.018
HR = 5.242 (1.132 - 24.278)
YTHDF2-high (n = 62)
YTHDF2-low (n = 62)
D
Age < 65 years
P = 0.01
HR = 5.882 (1.265 - 27.345)
YTHDF2-high (n = 52)
YTHDF2-low (n = 53)
E
Tumor T1/2/3
P = 0.025
HR = 3.915 (1.077 - 14.231)
YTHDF2-high (n = 65)
YTHDF2-low (n = 65)
F
Lymph node metastasis
P = 0.047
HR = 4.243 (0.898 - 20.028)
YTHDF2-high (n = 25)
YTHDF2-low (n = 25)
G
No distant metasitasis
P = 0.021
HR = 4.048 (1.113 - 14.719)
YTHDF2-high (n = 65)
YTHDF2-low (n = 65)
H
Stage I/II/III
P = 0.018
HR = 4.173 (1.147 - 15.181)
YTHDF2-high (n = 63)
YTHDF2-low (n = 63)

Figure 6. YTHDF2 predicts the PFS of patients with TNBC in TCGA dataset

(A) Number of samples in the whole cohort and different subgroups.
(B) Kaplan-Meier curves for PFS in all samples.
(C) Kaplan-Meier curves for PFS in age ≥40 years old subgroup.
(D) Kaplan-Meier curves for PFS in age <65 years old subgroup.
(E) Kaplan-Meier curves for PFS in tumor T1/2/3 subgroup.
(F) Kaplan-Meier curves for PFS in lymph node metastasis subgroup.
(G) Kaplan-Meier curves for PFS in negative distant metastasis subgroup.
(H) Kaplan-Meier curves for PFS in Stage I/II/III subgroup.

- *Ythdf2* small interfering RNA (siRNA) transfection
- Quantitative PCR (qPCR)
- Tumor cell suspension preparation and single-cell data mining
- Flow cytometry analysis
- MFI of $CFSE^+$ EMT6 cell assay
- Apoptosis assay
- Phagocytosis assay
- Clustering analysis of tumor-infiltrating immune cells and data visualization
- Annotation of cell clusters and differential expression analysis
- Prediction of macrophages and monocytes
- The discrimination of anti-tumoral and pro-tumoral macrophages
- Single cell pseudotime analysis
- Cell interaction analysis
- Transcription regulation network analysis
- Survival analysis

- QUANTIFICATION AND STATISTICAL ANALYSIS
- ADDITIONAL RESOURCES

SUPPLEMENTAL INFORMATION

Supplemental information can be found online at https://doi.org/10.1016/j.isci.2024.109902.

ACKNOWLEDGMENTS

This work was supported by grants from the National Science Foundation of China (82071859, 82371856, 82071860), Guangdong Natural Science Foundation (2020B1515120007), the Science and Technology Foundation of Guangdong Province (2021B1515230001), Guangdong Innovation and Entrepreneurship Team Projects (2019BT02Y198), Guangzhou Innovation and Entrepreneurship Team Projects (2024A03J1055) and Shanwei Innovation and Entrepreneurship Team Projects (2021A005, 2023A012, 2023A010).

AUTHOR CONTRIBUTIONS

H.J., Y.C., D.Z., and J.L. performed and analyzed multiple experiments. S.H., X.W., and W.D. performed specific experiments. J.H. and Y.Y. conceived ideas, supervised the work, and wrote the paper.

DECLARATION OF INTERESTS

There is no conflict of interest.

Received: December 24, 2023
Revised: March 11, 2024
Accepted: May 1, 2024
Published: May 3, 2024

REFERENCES

1. Bianchini, G., De Angelis, C., Licata, L., and Gianni, L. (2022). Treatment landscape of triple-negative breast cancer - expanded options, evolving needs. Nat. Rev. Clin. Oncol. *19*, 91–113. https://doi.org/10.1038/s41571-021-00565-2.
2. Cardoso, F., Kyriakides, S., Ohno, S., Penault-Llorca, F., Poortmans, P., Rubio, I.T., Zackrisson, S., and Senkus, E.; ESMO Guidelines Committee. Electronic address: clinicalguidelines@esmo.org (2019). Early breast cancer: ESMO clinical practice guidelines for diagnosis, treatment and follow-up. Ann. Oncol. *30*, 1194–1220. https://doi.org/10.1093/annonc/mdz173.
3. Vaduganathan, M., Claggett, B.L., Jhund, P.S., Cunningham, J.W., Pedro Ferreira, J., Zannad, F., Colleoni, M., Denkert, C., Piccart-Gebhart, M., Regan, M., et al. (2019). Estimating the benefits of therapy for early-stage breast cancer: the St. Gallen International Consensus Guidelines for the primary therapy of early breast cancer 2019.

Ann. Oncol. *30*, 1541–1557. https://doi.org/10.1093/annonc/mdz235.

4. Qiao, X., van der Zanden, S.Y., Wander, D.P.A., Borràs, D.M., Song, J.Y., Li, X., van Duikeren, S., van Gils, N., Rutten, A., van Herwaarden, T., et al. (2020). Uncoupling DNA damage from chromatin damage to detoxify doxorubicin. Proc. Natl. Acad. Sci. USA *117*, 15182–15192. https://doi.org/10.1073/pnas.1922072117.
5. van der Zanden, S.Y., Qiao, X., and Neefjes, J. (2021). New insights into the activities and toxicities of the old anticancer drug doxorubicin. FEBS J. *288*, 6095–6111. https://doi.org/10.1111/febs.15583.
6. Budd, G.T., Barlow, W.E., Moore, H.C.F., Hobday, T.J., Stewart, J.A., Isaacs, C., Salim, M., Cho, J.K., Rinn, K.J., Albain, K.S., et al. (2015). SWOG S0221: a phase III trial comparing chemotherapy schedules in high-risk early-stage breast cancer. J. Clin. Oncol. *33*, 58–64. https://doi.org/10.1200/JCO.2014.56.3296.
7. Foulkes, W.D., Smith, I.E., and Reis-Filho, J.S. (2010). Triple-negative breast cancer. N. Engl. J. Med. *363*, 1938–1948. https://doi.org/10.1056/NEJMra1001389.
8. Masuda, N., Lee, S.J., Ohtani, S., Im, Y.H., Lee, E.S., Yokota, I., Kuroi, K., Im, S.A., Park, B.W., Kim, S.B., et al. (2017). Adjuvant capecitabine for breast cancer after preoperative chemotherapy. N. Engl. J. Med. *376*, 2147–2159. https://doi.org/10.1056/NEJMoa1612645.
9. Cortazar, P., Zhang, L., Untch, M., Mehta, K., Costantino, J.P., Wolmark, N., Bonnefoi, H., Cameron, D., Gianni, L., Valagussa, P., et al. (2014). Pathological complete response and long-term clinical benefit in breast cancer: the CTNeoBC pooled analysis. Lancet *384*, 164–172. https://doi.org/10.1016/S0140-6736(13)62422-8.
10. Postow, M.A., Callahan, M.K., Barker, C.A., Yamada, Y., Yuan, J., Kitano, S., Mu, Z., Rasalan, T., Adamow, M., Ritter, E., et al. (2012). Immunologic correlates of the abscopal efect in a patient with melanoma. N. Engl. J. Med. *366*, 925–931. https://doi.org/10.1056/NEJMoa1112824.
11. Galluzzi, L., Buqué, A., Kepp, O., Zitvogel, L., and Kroemer, G. (2015). Immunological efects of conventional chemotherapy and targeted anticancer agents. Cancer Cell *28*, 690–714. https://doi.org/10.1016/j.ccell.2015.10.012.
12. De Palma, M., and Lewis, C.E. (2011). Cancer: Macrophages limit chemotherapy. Nature *472*, 303–304. https://doi.org/10.1038/472303a.
13. Cassetta, L., and Pollard, J.W. (2018). Targeting macrophages: therapeutic approaches in cancer. Nat. Rev. Drug Discov. *17*, 887–904. https://doi.org/10.1038/nrd.2018.169.
14. Mitchem, J.B., Brennan, D.J., Knolhoff, B.L., Belt, B.A., Zhu, Y., Sanford, D.E., Belaygorod, L., Carpenter, D., Collins, L., Piwnica-Worms, D., et al. (2013). Targeting tumor-infiltrating macrophages decreases tumor-initiating cells, relieves immunosuppression, and improves chemotherapeutic responses. Cancer Res. *73*, 1128–1141. https://doi.org/10.1158/0008-5472.CAN-12-2731.
15. Candas-Green, D., Xie, B., Huang, J., Fan, M., Wang, A., Menaa, C., Zhang, Y., Zhang, L., Jing, D., Azghadi, S., et al. (2020). Dual blockade of CD47 and HER2 eliminates radioresistant breast cancer cells. Nat. Commun. *11*, 4591. https://doi.org/10.1038/s41467-020-18245-7.
16. Locati, M., Curtale, G., and Mantovani, A. (2020). Diversity, mechanisms, and significance of macrophage plasticity. Annu. Rev. Pathol. *15*, 123–147. https://doi.org/10.1146/annurev-pathmechdis-012418-012718.
17. Rock, K.L., Reits, E., and Neefjes, J. (2016). Present Yourself! By MHC Class I and MHC Class II Molecules. Trends Immunol. *37*, 724–737. https://doi.org/10.1016/j.it.2016.08.010.
18. Neefjes, J., Jongsma, M.L.M., Paul, P., and Bakke, O. (2011). Towards a systems understanding of MHC class I and MHC class II antigen presentation. Nat. Rev. Immunol. *11*, 823–836. https://doi.org/10.1038/nri3084.
19. Mantovani, A., Allavena, P., Marchesi, F., and Garlanda, C. (2022). Tumour-associated macrophages as treatment targets in oncology. Nat. Rev. Drug Discov. *21*, 799–820. https://doi.org/10.1038/s41573-022-00520-5.
20. Bao, X., Shi, R., Zhao, T., Wang, Y., Anastasov, N., Rosemann, M., and Fang, W. (2021). Integrated analysis of single-cell RNA-seq and bulk RNA-seq unravels tumor heterogeneity plus M2-like tumour-associated macrophage infiltration and aggressiveness in TNBC. Cancer Immunol. Immunother. *70*, 189–202. https://doi.org/10.1007/s00262-020-02669-7.
21. Li, X., Ma, S., Deng, Y., Yi, P., and Yu, J. (2022). Targeting the RNA m6A modification for cancer immunotherapy. Mol. Cancer *21*, 76. https://doi.org/10.1186/s12943-022-01558-0.
22. Stoilov, P., Rafalska, I., and Stamm, S. (2002). YTH: a new domain in nuclear proteins. Trends Biochem. Sci. *27*, 495–497. https://doi.org/10.1016/s0968-0004(02)02189-8.
23. Dominissini, D., Moshitch-Moshkovitz, S., Schwartz, S., Salmon-Divon, M., Ungar, L., Osenberg, S., Cesarkas, K., Jacob-Hirsch, J., Amariglio, N., Kupiec, M., et al. (2012). Topology of the human and mouse m6A RNA methylomes revealed by m6A-seq. Nature *485*, 201–206. https://doi.org/10.1038/nature11112.
24. Wang, X., Lu, Z., Gomez, A., Hon, G.C., Yue, Y., Han, D., Fu, Y., Parisien, M., Dai, Q., Jia, G., et al. (2014). N6-methyladenosine-dependent regulation of messenger RNA stability. Nature *505*, 117–120. https://doi.org/10.1038/nature12730.
25. Chen, Y.G., Chen, R., Ahmad, S., Verma, R., Kasturi, S.P., Amaya, L., Broughton, J.P., Kim, J., Cadena, C., Pulendran, B., et al. (2019). N6-Methyladenosine Modification Controls Circular RNA Immunity. Mol. Cell *76*, 96–109.e9. https://doi.org/10.1016/j.molcel.2019.07.016.
26. Lin, Z., Wan, A.H., Sun, L., Liang, H., Niu, Y., Deng, Y., Yan, S., Wang, Q.P., Bu, X., Zhang, X., et al. (2023). N6-methyladenosine demethylase FTO enhances chemo-resistance in colorectal cancer through SIVA1-mediated apoptosis. Mol. Ther. *31*, 517–534. https://doi.org/10.1016/j.ymthe.2022.10.012.
27. Zhang, Y., Qiu, J.G., Jia, X.Y., Ke, Y., Zhang, M.K., Stieg, D., Liu, W.J., Liu, L.Z., Wang, L., and Jiang, B.H. (2023). METTL3-mediated N6-methyladenosine modification and HDAC5/YY1 promote IFFO1 downregulation in tumor development and chemo-resistance. Cancer Lett. *553*, 215971. https://doi.org/10.1016/j.canlet.2022.215971.
28. Ma, S., Sun, B., Duan, S., Han, J., Barr, T., Zhang, J., Bissonnette, M.B., Kortylewski, M., He, C., Chen, J., et al. (2023). YTHDF2 orchestrates tumor-associated macrophage reprogramming and controls antitumor immunity through CD8+ T cells. Nat. Immunol. *24*, 255–266. https://doi.org/10.1038/s41590-022-01398-6.
29. Hou, J., Zhang, H., Liu, J., Zhao, Z., Wang, J., Lu, Z., Hu, B., Zhou, J., Zhao, Z., Feng, M., et al. (2019). YTHDF2 reduction fuels inflammation and vascular abnormalization in hepatocellular carcinoma. Mol. Cancer *18*, 163. https://doi.org/10.1186/s12943-019-1082-3.
30. Meyer, K.D., and Jaffrey, S.R. (2017). Rethinking m6A Readers, Writers, and Erasers. Annu. Rev. Cell Dev. Biol. *33*, 319–342. https://doi.org/10.1146/annurev-cellbio-100616-060758.
31. Yan, J., and Horng, T. (2020). Lipid Metabolism in Regulation of Macrophage Functions. Trends Cell Biol. *30*, 979–989. https://doi.org/10.1016/j.tcb.2020.09.006.
32. Zhu, L., Zhao, Q., Yang, T., Ding, W., and Zhao, Y. (2015). Cellular metabolism and macrophage functional polarization. Int. Rev. Immunol. *34*, 82–100. https://doi.org/10.3109/08830185.2014.969421.
33. Wang, Y., Li, N., Zhang, X., and Horng, T. (2021). Mitochondrial metabolism regulates macrophage biology. J. Biol. Chem. *297*, 100904. https://doi.org/10.1016/j.jbc.2021.100904.
34. Joffe, A.M., Bakalar, M.H., and Fletcher, D.A. (2020). Macrophage phagocytosis assay with reconstituted target particles. Nat. Protoc. *15*, 2230–2246. https://doi.org/10.1038/s41596-020-0330-8.
35. Mass, E., Nimmerjahn, F., Kierdorf, K., and Schlitzer, A. (2023). Tissue-specific macrophages: how they develop and choreograph tissue biology. Nat. Rev. Immunol. *23*, 563–579. https://doi.org/10.1038/s41577-023-00848-y.
36. Salloum, G., Bresnick, A.R., and Backer, J.M. (2023). Macropinocytosis: mechanisms and regulation. Biochem. J. *480*, 335–362. https://doi.org/10.1042/BCJ20210584.
37. Bassez, A., Vos, H., Van Dyck, L., Floris, G., Arijs, I., Desmedt, C., Boeckx, B., Vanden Bempt, M., Nevelsteen, I., Lambein, K., et al. (2021). A single-cell map of intratumoral changes during anti-PD1 treatment of patients with breast cancer. Nat. Med. *27*, 820–832. https://doi.org/10.1038/s41591-021-01323-8.
38. Yunna, C., Mengru, H., Lei, W., and Weidong, C. (2020). Macrophage M1/M2 polarization. Eur. J. Pharmacol. *877*, 173090. https://doi.org/10.1016/j.ejphar.2020.173090.
39. Freud, A.G., Mundy-Bosse, B.L., Yu, J., and Caligiuri, M.A. (2017). The Broad Spectrum of Human Natural Killer Cell Diversity. Immunity *47*, 820–833. https://doi.org/10.1016/j.immuni.2017.10.008.
40. Väyrynen, J.P., Haruki, K., Lau, M.C., Väyrynen, S.A., Ugai, T., Akimoto, N., Zhong, R., Zhao, M., Dias Costa, A., Borowsky, J., et al. (2022). Spatial Organization and Prognostic Significance of NK and NKT-like Cells via Multimarker Analysis of the Colorectal Cancer Microenvironment. Cancer Immunol. Res. *10*, 215–227. https://doi.org/10.1158/2326-6066.CIR-21-0772.
41. Park, B., Heo, S.J., Lee, Y.J., Seo, M.K., Hong, J., Shin, E.C., Jung, I., and Kim, S. (2022). HLA-I-restricted CD8(+) T cell immunity may accelerate tumorigenesis in conjunction with VHL inactivation. iScience *25*, 104467. https://doi.org/10.1016/j.isci.2022.104467.

42. Ravindranath, M.H., Filippone, E.J., Devarajan, A., and Asgharzadeh, S. (2019). Enhancing Natural Killer and CD8(+) T Cell-Mediated Anticancer Cytotoxicity and Proliferation of CD8(+) T Cells with HLA-E Monospecific Monoclonal Antibodies. Monoclon. Antib. Immunodiagn. Immunother. *38*, 38–59. https://doi.org/10.1089/mab.2018.0043.
43. Wang, J., Jelcic, I., Mühlenbruch, L., Haunerdinger, V., Toussaint, N.C., Zhao, Y., Cruciani, C., Faigle, W., Naghavian, R., Foege, M., et al. (2020). HLA-DR15 Molecules Jointly Shape an Autoreactive T Cell Repertoire in Multiple Sclerosis. Cell *183*, 1264–1281.e20. https://doi.org/10.1016/j.cell.2020.09.054.
44. Sugata, K., Matsunaga, Y., Yamashita, Y., Nakatsugawa, M., Guo, T., Halabelian, L., Ohashi, Y., Saso, K., Rahman, M.A., Anczurowski, M., et al. (2021). Affinity-matured HLA class II dimers for robust staining of antigen-specific CD4(+) T cells. Nat. Biotechnol. *39*, 958–967. https://doi.org/10.1038/s41587-021-00836-4.
45. Pronier, E., Imanci, A., Selimoglu-Buet, D., Badaoui, B., Itzykson, R., Roger, T., Jego, C., Naimo, A., Francillette, M., Breckler, M., et al. (2022). Macrophage migration inhibitory factor is overproduced through EGR1 in TET2(low) resting monocytes. Commun. Biol. *5*, 110. https://doi.org/10.1038/s42003-022-03057-w.
46. Gharaibeh, L., Elmadany, N., Alwosaibai, K., and Alshaer, W. (2020). Notch1 in Cancer Therapy: Possible Clinical Implications and Challenges. Mol. Pharmacol. *98*, 559–576. https://doi.org/10.1124/molpharm.120.000006.
47. Zhang, J., Zhang, J., Zhao, W., Li, Q., and Cheng, W. (2022). Low expression of NR1H3 correlates with macrophage infiltration and indicates worse survival in breast cancer. Front. Genet. *13*, 1067826. https://doi.org/10.3389/fgene.2022.1067826.
48. Vanneste, D., Bai, Q., Hasan, S., Peng, W., Pirottin, D., Schyns, J., Maréchal, P., Ruscitti, C., Meunier, M., Liu, Z., et al. (2023). MafB-restricted local monocyte proliferation precedes lung interstitial macrophage differentiation. Nat. Immunol. *24*, 827–840. https://doi.org/10.1038/s41590-023-01468-3.
49. Gao, F., Alwhaibi, A., Artham, S., Verma, A., and Somanath, P.R. (2018). Endothelial Akt1 loss promotes prostate cancer metastasis via beta-catenin-regulated tight-junction protein turnover. Br. J. Cancer *118*, 1464–1475. https://doi.org/10.1038/s41416-018-0110-1.
50. Jiang, L., Wang, P., Song, X., Zhang, H., Ma, S., Wang, J., Li, W., Lv, R., Liu, X., Ma, S., et al. (2023). The HDAC2-SP1 Axis Orchestrates Protumor Macrophage Polarization. Cancer Res. *83*, 2345–2357. https://doi.org/10.1158/0008-5472.CAN-22-1270.
51. Langland, J.O., Cameron, J.M., Heck, M.C., Jancovich, J.K., and Jacobs, B.L. (2006). Inhibition of PKR by RNA and DNA viruses. Virus Res. *119*, 100–110. https://doi.org/10.1016/j.virusres.2005.10.014.
52. Lisci, M., Barton, P.R., Randzavola, L.O., Ma, C.Y., Marchingo, J.M., Cantrell, D.A., Paupe, V., Prudent, J., Stinchcombe, J.C., and Griffiths, G.M. (2021). Mitochondrial translation is required for sustained killing by cytotoxic T cells. Science *374*, eabe9977. https://doi.org/10.1126/science.abe9977.
53. Dolcet, X., Llobet, D., Pallares, J., and Matias-Guiu, X. (2005). NF-kB in development and progression of human cancer. Virchows Arch. *446*, 475–482. https://doi.org/10.1007/s00428-005-1264-9.
54. Zhang, G., Lu, J., Zheng, J., Mei, S., Li, H., Zhang, X., Ping, A., Gao, S., Fang, Y., and Yu, J. (2024). Spi1 regulates the microglial/macrophage inflammatory response via the PI3K/AKT/mTOR signaling pathway after intracerebral hemorrhage. Neural Regen. Res. *19*, 161–170. https://doi.org/10.4103/1673-5374.375343.
55. Jiang, L., Wang, P., Song, X., Zhang, H., Ma, S., Wang, J., Li, W., Lv, R., Liu, X., Ma, S., et al. (2021). Salmonella Typhimurium reprograms macrophage metabolism via T3SS effector SopE2 to promote intracellular replication and virulence. Nat. Commun. *12*, 879. https://doi.org/10.1038/s41467-021-21186-4.
56. Basha, S., Jin-Smith, B., Sun, C., and Pi, L. (2023). The SLIT/ROBO Pathway in Liver Fibrosis and Cancer. Biomolecules *13*, 785. https://doi.org/10.3390/biom13050785.
57. Yang, Z., Huo, Y., Zhou, S., Guo, J., Ma, X., Li, T., Fan, C., and Wang, L. (2022). Cancer cell-intrinsic XBP1 drives immunosuppressive reprogramming of intratumoral myeloid cells by promoting cholesterol production. Cell Metab. *34*, 2018–2035.e8. https://doi.org/10.1016/j.cmet.2022.10.010.
58. Zhao, Y., Zhang, W., Huo, M., Wang, P., Liu, X., Wang, Y., Li, Y., Zhou, Z., Xu, N., and Zhu, H. (2021). XBP1 regulates the protumoral function of tumor-associated macrophages in human colorectal cancer. Signal Transduct. Target. Ther. *6*, 357. https://doi.org/10.1038/s41392-021-00761-7.
59. Zhou, Y., Xu, J., Luo, H., Meng, X., Chen, M., and Zhu, D. (2022). Wnt signaling pathway in cancer immunotherapy. Cancer Lett. *525*, 84–96. https://doi.org/10.1016/j.canlet.2021.10.034.
60. Li, Y.Q., Sun, F.Z., Li, C.X., Mo, H.N., Zhou, Y.T., Lv, D., Zhai, J.T., Qian, H.L., and Ma, F. (2023). RARRES2 regulates lipid metabolic reprogramming to mediate the development of brain metastasis in triple negative breast cancer. Mil. Med. Res. *10*, 34. https://doi.org/10.1186/s40779-023-00470-y.
61. Carvalho, R.F., do Canto, L.M., Abildgaard, C., Aagaard, M.M., Tronhjem, M.S., Waldstrøm, M., Jensen, L.H., Steffensen, K.D., and Rogatto, S.R. (2022). Single-cell and bulk RNA sequencing reveal ligands and receptors associated with worse overall survival in serous ovarian cancer. Cell Commun. Signal. *20*, 176. https://doi.org/10.1186/s12964-022-00991-4.
62. Ni, Y., Zhuge, F., Ni, L., Nagata, N., Yamashita, T., Mukaida, N., Kaneko, S., Ota, T., and Nagashimada, M. (2022). CX3CL1/CX3CR1 interaction protects against lipotoxicity-induced nonalcoholic steatohepatitis by regulating macrophage migration and M1/M2 status. Metabolism *136*, 155272. https://doi.org/10.1016/j.metabol.2022.155272.
63. Ademuyiwa, F.O., Chen, I., Luo, J., Rimawi, M.F., Hagemann, I.S., Fisk, B., Jeffers, G., Skidmore, Z.L., Basu, A., Richters, M., et al. (2021). Immunogenomic profiling and pathological response results from a clinical trial of docetaxel and carboplatin in triple-negative breast cancer. Breast Cancer Res. Treat. *189*, 187–202. https://doi.org/10.1007/s10549-021-06307-3.
64. Wang, T., Jin, H., Hu, J., Li, X., Ruan, H., Xu, H., Wei, L., Dong, W., Teng, F., Gu, J., et al. (2020). COL4A1 promotes the growth and metastasis of hepatocellular carcinoma cells by activating FAK-Src signaling. J. Exp. Clin. Cancer Res. *39*, 148. https://doi.org/10.1186/s13046-020-01650-7.
65. Chen, H., Sun, Q., Zhang, C., She, J., Cao, S., Cao, M., Zhang, N., Adiila, A.V., Zhong, J., Yao, C., et al. (2021). Identification and Validation of CYBB, CD86, and C3AR1 as the Key Genes Related to Macrophage Infiltration of Gastric Cancer. Front. Mol. Biosci. *8*, 756085. https://doi.org/10.3389/fmolb.2021.756085.
66. Li, R., Zeng, L., Zhao, H., Deng, J., Pan, L., Zhang, S., Wu, G., Ye, Y., Zhang, J., Su, J., et al. (2022). ATXN2-mediated translation of TNFR1 promotes esophageal squamous cell carcinoma via m6A-dependent manner. Mol. Ther. *30*, 1089–1103. https://doi.org/10.1016/j.ymthe.2022.01.006.
67. Yao, J., Zhang, Y., Li, M., Sun, Z., Liu, T., Zhao, M., and Li, Z. (2021). Single-Cell RNA-Seq Reveals the Promoting Role of Ferroptosis Tendency During Lung Adenocarcinoma EMT Progression. Front. Cell Dev. Biol. *9*, 822315. https://doi.org/10.3389/fcell.2021.822315.
68. Yang, P., Qin, H., Li, Y., Xiao, A., Zheng, E., Zeng, H., Su, C., Luo, X., Lu, Q., Liao, M., et al. (2022). CD36-mediated metabolic crosstalk between tumor cells and macrophages affects liver metastasis. Nat. Commun. *13*, 5782. https://doi.org/10.1038/s41467-022-33349-y.
69. Theruvath, J., Menard, M., Smith, B.A.H., Linde, M.H., Coles, G.L., Dalton, G.N., Wu, W., Kiru, L., Delaidelli, A., Sotillo, E., et al. (2022). Anti-GD2 synergizes with CD47 blockade to mediate tumor eradication. Nat. Med. *28*, 333–344. https://doi.org/10.1038/s41591-021-01625-x.
70. Casazza, A., Laoui, D., Wenes, M., Rizzolio, S., Bassani, N., Mambretti, M., Deschoemaeker, S., Van Ginderachter, J.A., Tamagnone, L., and Mazzone, M. (2013). Impeding macrophage entry into hypoxic tumor areas by Sema3A/Nrp1 signaling blockade inhibits angiogenesis and restores antitumor immunity. Cancer Cell *24*, 695–709. https://doi.org/10.1016/j.ccr.2013.11.007.
71. Polavaram, N.S., Dutta, S., Islam, R., Bag, A.K., Roy, S., Poitz, D., Karnes, J., Hofbauer, L.C., Kohli, M., Costello, B.A., et al. (2021). Tumor- and osteoclast-derived NRP2 in prostate cancer bone metastases. Bone Res. *9*, 24. https://doi.org/10.1038/s41413-021-00136-2.
72. Fang, R., Chen, X., Zhang, S., Shi, H., Ye, Y., Shi, H., Zou, Z., Li, P., Guo, Q., Ma, L., et al. (2021). EGFR/SRC/ERK-stabilized YTHDF2 promotes cholesterol dysregulation and invasive growth of glioblastoma. Nat. Commun. *12*, 177. https://doi.org/10.1038/s41467-020-20379-7.
73. Li, J., Xie, H., Ying, Y., Chen, H., Yan, H., He, L., Xu, M., Xu, X., Liang, Z., Liu, B., et al. (2020). YTHDF2 mediates the mRNA degradation of the tumor suppressors to induce AKT phosphorylation in N6-methyladenosine-dependent way in prostate cancer. Mol. Cancer *19*, 152. https://doi.org/10.1186/s12943-020-01267.
74. Yu, Z., Guo, J., Hu, M., Gao, Y., and Huang, L. (2020). Icaritin Exacerbates Mitophagy and Synergizes with Doxorubicin to Induce Immunogenic Cell Death in Hepatocellular Carcinoma. ACS Nano *14*, 4816–4828. https://doi.org/10.1021/acsnano.0c00708.
75. Zierhut, C., Yamaguchi, N., Paredes, M., Luo, J.D., Carroll, T., and Funabiki, H. (2019). The Cytoplasmic DNA Sensor cGAS Promotes

Mitotic Cell Death. Cell *178*, 302–315.e23. https://doi.org/10.1016/j.cell.2019.05.035.

76. Cullis, J., Siolas, D., Avanzi, A., Barui, S., Maitra, A., and Bar-Sagi, D. (2017). Macropinocytosis of Nab-paclitaxel Drives Macrophage Activation in Pancreatic Cancer. Cancer Immunol. Res. *5*, 182–190. https://doi.org/10.1158/2326-6066.CIR-16-0125.

77. Wang, Q.S., Gao, L.N., Zhu, X.N., Zhang, Y., Zhang, C.N., Xu, D., and Cui, Y.L. (2019). Co-delivery of glycyrrhizin and doxorubicin by alginate nanogel particles attenuates the activation of macrophage and enhances the therapeutic efficacy for hepatocellular carcinoma. Theranostics *9*, 6239–6255. https://doi.org/10.7150/thno.35972.

78. Hao, Y., Hao, S., Andersen-Nissen, E., Mauck, W.M., Zheng, S., Butler, A., Lee, M.J., Wilk, A.J., Darby, C., Zager, M., et al. (2021). Integrated analysis of multimodal single-cell data. Cell *184*, 3573–3587.e29. https://doi.org/10.1016/j.cell.2021.04.048.

79. Street, K., Risso, D., Fletcher, R.B., Das, D., Ngai, J., Yosef, N., Purdom, E., and Dudoit, S. (2018). Slingshot: cell lineage and pseudotime inference for single-cell transcriptomics. BMC Genom. *19*, 477. https://doi.org/10.1186/s12864-018-4772-0.

80. Jin, S., Guerrero-Juarez, C.F., Zhang, L., Chang, I., Ramos, R., Kuan, C.H., Myung, P., Plikus, M.V., and Nie, Q. (2021). Inference and analysis of cellcell communication using CellChat. Nat. Commun. *12*, 1088. https://doi.org/10.1038/s41467-021-21246-9.

81. Bravo González-Blas, C., De Winter, S., Hulselmans, G., Hecker, N., Matetovici, I., Christiaens, V., Poovathingal, S., Wouters, J., Aibar, S., Aerts, S., et al. (2023). SCENIC+: single-cell multiomic inference of enhancers and gene regulatory networks. Nat. Methods *20*, 1355–1367. https://doi.org/10.1038/s41592-023-01938-4.

82. Zhang, Y., Chen, H., Mo, H., Hu, X., Gao, R., Zhao, Y., Liu, B., Niu, L., Sun, X., Yu, X., et al. (2021). Single-cell analyses reveal key immune cell subsets associated with response to PD-L1 blockade in triple-negative breast cancer. Cancer Cell *39*, 1578–1593.e8. https://doi.org/10.1016/j.ccell.2021.09.010.

STAR★METHODS

KEY RESOURCES TABLE

REAGENT or RESOURCE	SOURCE	IDENTIFIER
Antibodies		
BV421-*anti*-F4/80	BD, America	Cat# 565411; RRID:AB_2734779
PE-Cy7-*anti*-Cd11b	BD, America	Cat# 552850; RRID:AB_394491
FITC-*anti*-Cd80	BD, America	Cat# 561954; RRID:AB_10896321
BV650-*anti*-Cd86	BD, America	Cat# 564200; RRID:AB_2738665
Alexa 647-*anti*-Cd206	BD, America	Cat# 565250; RRID:AB_2739133
BV605-*anti*-F4/80	BioLegend, America	Cat# 123133, RRID:AB_2562305
CFSE	Biolegend, America	Cat# 423801, RRID:AB_2869649
Annexin V-APC/7-AAD	AB Science, France	Cat# E-CK-A218, RRID:AB_2869266
Critical commercial assays		
DMEM	Thermo Fisher Scientific, America	Cat# 11965092
LPS	Sigma-Aldrich, USA	Cat# 297-473-0
IL-4	Thermo Fisher Scientific, Peprotech, America	Cat # 214-14-5UG
Trypsin-EDTA (0.25%), containing phenol red	Thermo Fisher Scientific, America	Cat# 25200056
Fetal Bovine Serum, Premium Plus, heat	Thermo Fisher Scientific, Canada	Cat# A3160801-1
Penicillin-streptomycin (10,000 U/mL)	Thermo Fisher Scientific, America	Cat# 15140122
Alanyl-glutamine (GlutaMAX) (200mM),100×	Procell, China	Cat# PB180419
DMSO (Dimethyl sulfoxide)	Solarbio, China	Cat# D8371-50
RNA Quick Purification kit	HaiGene, China	Cat# B0132
Hifair® III 1st Strand cDNA Synthesis SuperMix	YEASEN, China	Cat# 11141ES60
Hieff SYBR Green Master Mix	YEASEN, China	Cat# 11199ES03
384 well white PCR plate	LABTIDE, China	Cat# 60384
Fixable Viability Stain 700	BDbiosciences, America	Cat# 564997
Fixation/Permeablization Kit	BDbiosciences, America	Cat# 554714
siRNA against *Ythdf2*	Golden Transfer Technology, China	Cat# R19425010
non-targeting siNC	Genepharma, China	Cat# A06001
Deposited data		
Single cell RNA-seq data	*This paper*	GSE263995
Single cell RNA-seq data	GEO	GSE169246
Software and algorithms		
R (v4.2.3)	The R Foundation	https://www.r-project.org
Seurat (v4.3.0.1, R package)	Hao et al.[78]	https://satijalab.org/seurat/index.html
Slingshot (v2.6.0, R package)	Street et al.[79]	Bioconductor
CellChat (v1.6.1, R package)	Jin et al.[80]	https://github.com/sqjin/CellChat
SCENIC (v1.3.1, R package)	Bravo González-Blas et al.[81]	Bioconductor

RESOURCE AVAILABILITY

Lead contact

Further information and requests for resources and reagents should be directed to and will be fulfilled by the lead contact.

Materials availability

This study did not generate new unique reagents.

Data and code availability

Raw data and processed, de-identified scRNA-seq gene expression datasets generated during this study is deposited and publically available at the Gene Expression Omnibus (GEO) with the accession number GSE263995, as listed in the key resources table. This paper also analyzes existing, publicly available data. The accession number for this dataset is listed in the key resources table.

This paper does not report original code. Any additional information required to reanalyze the data reported in this paper is available from the lead contact upon request.

EXPERIMENTAL MODEL AND STUDY PARTICIPANT DETAILS

Animal subjects

C57BL/6J female mice were purchased from BesTest Biotech Co.Ltd (Zhuhai, China) and raised at the Laboratory Animal Resource Center of Sun Yat-sen University (Guangzhou, China). They were bred and maintained under pathogen-free conditions with free access to food and water. Mice were ready at the age of 6–7 weeks. All experiments were meticulously conducted under the instruction from the Sun Yat-Sen University Laboratory Animal Care and Use Committee.

Human subjects

Chemotherapy-naive and post-chemotherapy invasive breast cancer samples were obtained from two patients from Sun Yat-sen Memorial Hospital. Patients were at an average age of 50.5 years (+/−6.36 years) and both female. Informed consents had been obtained from both participants, and all related procedures were performed with the approval of the Internal Review and Ethics Boards of Sun Yat-sen Memorial Hospital. The Approval Number was SYSKY-2023-1210-01.

METHOD DETAILS

Patients and sample collection

These analyses were based on the single-cell RNA sequencing (scRNA-seq) performed in this study and publicly available data (GSE169246).[82] Two patients diagnosed with TNBC (P01, $cT_2N_1M_0$; P02, $cT_1N_1M_0$) who received the cyclophosphamide (600 mg/m^2) plus doxorubicin (90 mg/m^2) regimen (on Day 1 of every 21-day cycle) of chemotherapy were eligible for enrollment and they achieved CR. Collected breast tumor specimens from pre/post-treatment biopsies were reserved in tissue storage solution and subjected to scRNA-seq in a timely manner.

The public available scRNA-seq data were referenced from GSE169246.[82] The dataset enrolled five patients with TNBC receiving the paclitaxel (90 mg/m^2) regimen (on Days 1/8/15 of every 28-day cycle) of NAC. Two of them (GSEP020, $cT_2N_2M_0$; GSEP022, $cT_2N_2M_1$, 44.5 $\pm$ 14.85 years, both female) achieved PR, while the other three (GSEP018, $cT_2N_2M_0$; GSEP023, $cT_2N_2M_0$; GSEP025, $cT_2N_1M_0$, 45.0 $\pm$ 7.55 years, all female) achieved SD after chemotherapy. The dataset also provided their pre/post-treatment scRNA-seq data.[82]

For patients from our study and GSE169246 dataset, the clinical efficacy of chemotherapy was evaluated based on the volume reduction rate (VRR) of the original breast tumor at a time point of eight weeks status post chemotherapy: CR: VRR >90%; PR: 90% > VRR >30%; SD: 30% > VRR > −30%.

Cell culture and macrophage polarization

BMDMs were cultured in DMEM containing 10% fetal bovine serum (FBS, heat-inactivated) and penicillin-streptomycin antibiotics (both 50 μg/mL). The medium was incubated at 37°C and 5% CO_2. The cells were then seeded into 6-well plates (1×10^5/well) and treated with either LPS (1 μg/mL) or murine IL-4 (20 ng/mL) for 12 h in order to generate anti-tumoral or pro-tumoral macrophages, respectively.

Ythdf2 small interfering RNA (siRNA) transfection

BMDMs (1×10^5/well) were seeded into 6-well plates with 2 mL DMEM and cultured for 24 h at 37°C and 5% CO_2. Cells with 70% or higher confluency were selected for transfection. In the experimental group, cells were transfected with 40 nM siRNA against *Ythdf2*, while the control group received non-targeting siNC. This enabled the knockdown of *Ythdf2* expression in the experimental group. A total of three siRNA sequences (these sequences are shown in Table S1) targeting mouse *Ythdf2* genes were prepared in this study.

Quantitative PCR (qPCR)

RNAs were isolated using the RNA Quick Purification kit and then reversely transcribed to cDNA using a PrimeScript RT reagent kit with gDNA Eraser following the manufacturer's instructions. The levels of mRNA expression were analyzed using the SYBR Green PCR master mix and detected by a LightCycler 480 thermal cycler (Roche, Basel, Switzerland). The sequences of all primers are displayed in Table S2.

Tumor cell suspension preparation and single-cell data mining

Biopsied tissues were immersed in tissue protection solution and kept on ice during transportation. In the lab, tissues were transferred to a 50 mL centrifuge tube, washed with 10 mL 1 x HBSS, and then placed on a culture dish without HBSS. After removing any residual blood, tissues were minced into small pieces and digested at 37°C for 30 min in a warm water bath. Digestive reagents consisted of 0.1% (1 mg/mL) collagenase, 0.1% (1 mg/mL) neural protease, 0.02% (0.2 mg/mL) DNase I, and 2.5 mL DMEM. The digestion process was terminated using

complete DMEM medium. Then we filtered the digested mixture through a 100 μm sieve and centrifuged at 4°C with 350 g for 5 min. We used 1 mL pre-cooled 1 x Red Blood Cell Removal Solution to carefully remove red blood cells. The suspension was filtered through a 40 μm sieve, and the cell number was counted using a Bio-Rad TC20 cell counting machine. The suspension was then diluted with HBSS to achieve a concentration of 700–1200 cells/μL. It subsequently underwent single-cell sequencing using 10×Genomics within 30 min of preparation. Single-cell sequencing data of PR and SD cohorts were referenced from the dataset GSE169246.[82]

Flow cytometry analysis

After adding the desired combination of fluorochrome-conjugated antibodies (Anti-tumoral marker flow dyes included BV421-*anti*-F4/80, PE-Cy7-*anti*-Cd11b, FITC-*anti*-Cd80 and BV650-*anti*-Cd86; Pro-tumoral marker flow dyes included BV421-*anti*-F4/80, PE-Cy7-*anti*-Cd11b and Alexa 647-*anti*-Cd206), the BMDMs to be tested were incubated on ice for 30 min in the dark. Thereafter, the BMDMs were subjected to flow cytometry analysis. Data were analyzed with FlowJo Software.

MFI of CFSE$^+$ EMT6 cell assay

EMT6 cells were labeled with CFSE cell proliferation dye according to the manufacturer's instructions. Briefly, CFSE stocksolution was diluted with PBS to a working solution of 0.2muM. Cells were resuspended in pre-warmed CFSE working solution and incubated at 37°C for 15min in the incubator. Cells were pelleted by centrifugation, resuspended in pre-warmed (37°C) RPMI medium and incubated at 37°C for 30 min. Cells were then pelleted and resuspended inmedium to a density of 4×10^5 cells/mL. BMDMs were pretreated with either siRNA^{Ythdf2} or non-targeting siRNA. Labeled EMT6 cells were added to the plate containing BMDMs at a cell ratio of 4:1. The EMT6-BMDM mixtures were cultured in the CO_2 incubator. Culture supernatant was collected after respectively 12 h and 24 h. Adherent EMT6 cells were harvested using 0.05% Trypsin-EDTA solution and combined with the cultured supernatant. The collected EMT6 cell and BMDM mixtures was pelleted by centrifugation, resuspended in PBS. Cells were analyzed immediately by flow cytometry. The MFI of CFSE$^+$ EMT6 cells was analyzed by flow cytometry to reveal the proliferation rate of CFSE$^+$ EMT6 cells.

Apoptosis assay

EMT6 cells were labeled with CFSE. Then, EMT6 cells (4×10^5) were added to the plate containing BMDMs at a cell ratio of 4:1. After incubation for 12 h, apoptosis of EMT6 cells were assessed using the Annexin V-APC/7-AAD Apoptosis Detection Kit.

Phagocytosis assay

EMT6 cells were labeled with CFSE. Then, the labeled EMT6 cells (4×10^5) were added to the plate containing BMDMs at a cell ratio of 4:1. After incubation for 24 h, the BMDMs were labeled with BV605−F4/80$^+$. Subsequently, the phagocytosis of macrophages was assessed based on the percentages of dual-positive macrophages (CFSE$^+$/BV605$^+$) in the total macrophage population (BV605$^+$) analyzed by flow cytometry.

Clustering analysis of tumor-infiltrating immune cells and data visualization

We fed the obtained UMI count matrix into Seurat (v4.3.0.1, R package)[78] for further processing. We applied 'NormalizeData' function with default parameters to normalize the gene expression level in each single cell for all the three datasets. Next, we identified 2,000 highly variable genes using the 'FindVariableFeatures' functionwith 'vst' method. We used the 'ScaleData' function to scale and center gene expression matrices. The first 15 principal components were selected to construct the shared nearest neighbor (SNN) graph with 'FindNeighbors' function, and then clusters were determined using the Louvain algorithm. Cluster resolution was set as 0.5 based on the principle that each cell cluster should express a unique group of genes. After clustering was completed, the ones with high variable mitochondrial contamination genes (*MT-[X]* genes) and ribosomal contamination genes (*RPL/RPS[X]* genes) were discarded. We applied the uniform manifold approximation and projection (UMAP) based on the SNN graph acquired above to visualize the single cell profile.

Annotation of cell clusters and differential expression analysis

We adopted the 'FindAllMarkers' function of Seurat package with min.pct = 0.3 to identify differentially expressed genes in each cluster. If a representative marker gene of a particular immune cell type ranked on top of the list for a query cluster, we would accordingly assign the most likely identity for this cluster.

Prediction of macrophages and monocytes

Given the similarities of transcriptomic profiles shared by macrophages and monocytes, the distinction of the two cell types based on the solitary cell clustering will be challenging. We hereby utilized the expressions of macrophage marker genes (*C1QB*, *CXCL8*, and *SPP1*) to better identify macrophages.

The discrimination of anti-tumoral and pro-tumoral macrophages

We imported the obtained scRNA-seq data of macrophages into computational procedures. Using the 'FindVariableFeatures' algorithm in Seurat Package, over 2,000 highly variable genes were identified. Close attentions were paid on the anti-tumoral phenotype marker genes

including *IL1B*, *NFKB1*, *TNF*, and pro-tumoral marker genes including *CD163*, *MRC1*, *APOE* as the determinants to discriminate the two subtypes of macrophages.

Single cell pseudotime analysis

We applied Slingshot (v2.6.0, R package)[79] to identify the imputed pseudotime trajectory in tumor anti-tumoral and pro-tumoral macrophages. The UMAP matrix obtained from the above clustering analysis was fed into 'slingshot' function.

Cell interaction analysis

We employed the annotated Seurat package to construct cell interaction networks. CellChat (v1.6.1, R package)[80] was applied for inferring and visualizing the intracellular communication based on the expressions of known ligand-receptor pairs. The expression matrix and cell types were extracted. The interactions between different cell types were characterized by a ligand-receptor database. Subsets were created to identify over-expressed genes and ligand-receptor pairs. The common probabilities of intercellular interactions were subsequently calculated. The evaluations of the communications between macrophages and all other immune cell categories in *YTHDF2*-low and *YTHDF2*-high groups were firstly performed, followed by the scrutiny of significantly correlated cell types.

Transcription regulation network analysis

The expression matrix was used to calculate the correlative strength between TFs and genes. We adopted SCENIC (v1.3.1 R package)[81] to identify critical TFs for *YTHDF2*-low and *YTHDF2*-high macrophages. Information on motifs was obtained from gene databases. The levels of gene expression determined their ranks, with the top 5% selected for AUC calculation. We scaled the AUC value by the expression levels of *YTHDF2*. Activated TFs were identified based on the AUC value; higher ranks of genes indicate stronger activities of their corresponding TFs.

Survival analysis

The *YTHDF2*-related geneset was downloaded from the GENECARD dataset. Clinical and genomic data of patients with TNBC were referenced from TCGA dataset. Based on the average expression value of each gene in the geneset, we classified the patients into two groups (*YTHDF2*-high and *YTHDF2*-low groups) and examined their prognoses. The prognosis of each group of patients was examined by Kaplan-Meier survival estimators, and the survival outcomes of the two groups were compared by log rank tests. The survival outcomes with significant difference were examined and we selected the value which yields the lowest log rank *p* value to be the best cutoff value of the two groups.

QUANTIFICATION AND STATISTICAL ANALYSIS

Data shown represents the number of human $CD45^+$ immune cells or macrophages derived from the number of indicated independent donors, or independent BMDM preparations for mouse *in vitro* studies. Pooled data was analyzed by SPSS 26.0 and Figures generated in Graph Pad Prism. Two-sided t test was carried out on *in vitro* experiments to indicate significant differences between treatment groups or conditions as indicated in Figures. For comparisons of the *YTHDF2* or pro-tumoral/anti-tumoral marker gene expression levels between 2 groups, Moses Extreme Reactions test was performed. * indicates comparisons $p < 0.05$ between two groups. ** indicates comparisons $p < 0.01$ between two groups. *** indicates comparisons $p < 0.001$ between two groups.

ADDITIONAL RESOURCES

This work is a part of a clinical trial (clinical registry number ChiCTR2100041675, associated links https://www.chictr.org.cn/showproj.html?proj=66604).